*Inorg. Chem.* **2006**, *45*, 3224–3239

# Structural Diversity of the Oxovanadium Organodiphosphonate System: A Platform for the Design of Void Channels

**Wayne Ouellette,[†] Ming Hui Yu,[‡] Charles J. O'Connor,[‡] and Jon Zubieta*[,†]**

*Department of Chemistry, Syracuse University, Syracuse, New York 13244, and Advanced Materials Research Institute, University of New Orleans, New Orleans, Louisiana 70148*

Received October 7, 2005

The hydrothermal reactions of a vanadium source, an appropriate diphosphonate ligand, and water in the presence of HF provide a series of compounds with neutral V–P–O networks as the recurring structural motif. When the $\{O_3P(CH_2)_nPO_3\}^{4-}$ diphosphonate tether length $n$ is 2–5, metal–oxide hybrids of type **1**, $[V_2O_2(H_2O)\{O_3P(CH_2)_n$-$PO_3\}]\cdot xH_2O$, are isolated. The type **1** oxides exhibit the prototypical three-dimensional (3-D) "pillared" layer architecture. When $n$ is increased to 6–8, the two-dimensional (2-D) "pillared" slab structure of the type **2** oxides $[V_2O_2(H_2O)_4$-$\{O_3P(CH_2)_6PO_3\}]$ is encountered. Further lengthening of the spacer to $n = 9$ provides another 3-D structure, type **3**, constructed from the condensation of pillared slabs to give V–P–O double layers as the network substructure. When organic cations are introduced to provide charge balance for anionic V–P–O networks, oxides of types **4**–**7** are observed. For spacer length $n = 3$, a range of organodiammonium cations are accommodated by the same 3-D "pillared" layer oxovanadium diphosphonate framework in the type **4** materials $[H_3N(CH_2)_nNH_3][V_4O_4(OH)_2$ $\{O_3P(CH)_3PO_3\}_2]\cdot xH_2O$ [$n = 2$, $x = 6$ (**4a**); $n = 3$, $x = 3$ (**4b**); $n = 4$, $x = 2$ (**4c**); $n = 5$, $x = 1$ (**4d**); $n = 6$, $x = 0.5$ (**4e**); $n = 7$, $x = 0$ (**4f**)] and $[H_3NR]_y[V_4O_4(OH)_2$ $\{O_3P(CH)_3PO_3\}_2]\cdot xH_2O$ [R = $-CH_2(NH_3)CH_2CH_3$, $y = 1$, $x = 0$ (**4g**); R = $-CH_3$, $n = 2$, $x = 3$ (**4h**); R = $-CH_2CH_3$, $y = 2$, $x = 1$ (**4i**); R = $-CH_2CH_2CH_3$, $y = 2$, $x = 0$ (**4j**); cation = $[H_2N(CH_2CH_3)_2]$, $y = 2$, $x = 0$ (**4k**)]. These oxides exhibit two distinct interlamellar domains, one occupied by the cations and the second by water of crystallization. Furthermore, as the length of the cation increases, the organodiammonium component spills over into the hydrophilic domain to displace the water of crystallization. When the diphosphonate tether length is increased to $n = 5$, structure type **5**, $[H_3N(CH_2)_2NH_3]$-$[V_4O_4(OH)_2(H_2O)\{O_3P(CH_2)_5PO_3\}_2]\cdot H_2O$, is obtained. This oxide possesses a 2-D "pillared" network or slab structure, similar in gross profile to that of type **2** oxides and with the cations occupying the interlamellar domain. In contrast, shortening the diphosphonate tether length to $n = 2$ results in the 3-D oxovanadium organophosphonate structure of the type **7** oxide $[H_3N(CH_2)_5NH_3][V_3O_3\{O_3P(CH_2)_2PO_3\}_2]$. The ethylenediphosphonate ligand does not pillar V–P–O networks in this instance but rather chelates to a vanadium center in the construction of complex polyhedral connectivity of **7**. Substitution of piperazinium cations for the simple alkyl chains of types **4**, **5**, and **7** provides the 2-D pillared layer structure of the type **6** oxides, $[H_2N(CH_2CH_2)NH_2][V_2O_2\{O_3P(CH)_nPO_3H\}_2]$ [$n = 2$ (**6a**); $n = 4$ (**6b**); $n = 6$ (**6c**)]. The structural diversity of the system is reflected in the magnetic properties and thermal behavior of the oxides, which are also discussed.

The significant contemporary interest in the rational design of new oxide materials reflects their vast compositional range, structural diversity, extensive physical properties, and important applications.[1−4] The oxovanadium phosphate system (V−P−O or VOPO) has been extensively developed for catalytic applications, most specifically the remarkable selective air oxidation of butane to maleic anhydride by

* To whom correspondence should be addressed. E-mail: jazubiet@syr.edu. Telefax: international code + (315) 443-4070.

[†] Syracuse University.

[‡] University of New Orleans.

(1) McCarroll, W. H. In *Encyclopedia of Inorganic Compounds*; King, R. B., Ed.; John Wiley & Sons: New York, 1994; Vol. 6, pp 2903−2946.

(2) Cheetham, A. K. *Science* **1994**, *264*, 794.

(3) Bruce, D. W., O'Hare, D., Eds. *Inorganic Materials*; Wiley: Chichester, U.K., 1992.

(4) Fierro, J. L. G., Ed. *Metal Oxides: Chemistry and Applications*; CRC Press: Boca Raton, FL, 2005.



10.1021/ic0517422 CCC: $33.50 
Published on Web 03/07/2006

vanadyl pyrophosphate and vanadyl phosphite.[5−8] Furthermore, the V−P−O system exhibits considerable structural and compositional variety,[9] reflecting the variable oxidation states and coordination polyhedra accessible to the vanadium center, the ability of vanadium polyhedra to aggregate into oligomers or chain or network $\{V_xO_y\}_n^{m-}$ substructures, the accessible range of vanadium and phosphorus polyhedral connectivities, and the possibility of protonation of oxygen sites and coordination of aqua ligands.

The structural diversity of the V−P−O system may be further elaborated by organic modification of the phosphate component to provide an organophosphonate building block $\{O_3PR\}$. Metal organophosphonates represent an important subclass of the metal−oxides, both in terms of applications to areas as diverse as catalysis, proton conductivity, ion exchange, intercalation chemistry, and photochemistry and as prototypical organic/inorganic hybrid materials.[10,11] More specifically, vanadyl organophosphonates possess structurally well-defined internal void spaces,[12,13] which allow the materials to intercalate substrates, to act as potential storage devices, and to find use as hybrid composite materials in electrooptical applications.[14] The advantages of the oxovanadium organophosphonates in applications to the synthetic design of porous materials[15,16] include the thermal stability of the metal−oxide V−P−O substructure, readily modified organic substituents, the interplay of hydrophilic and hydrophobic domains, and in certain cases the actual or incipient coordinative unsaturation of the vanadium sites.

**Chart 1**

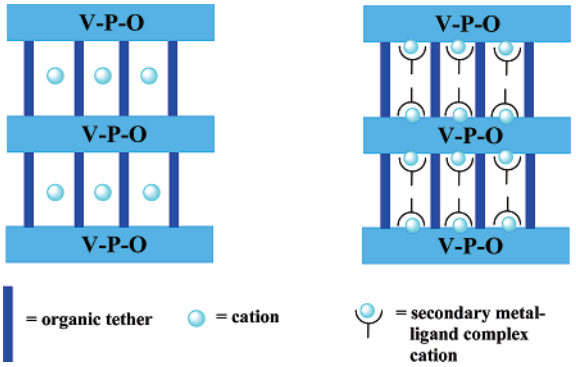


While the oxovanadium organophosphonates exhibit a range of structures,[9] including molecular clusters, chains, layers, and three-dimensional (3-D) frameworks, the two-dimensional (2-D) network of V−P−O layers separated by hydrophobic organic domains is the most common type (Chart 1). Investigations of the oxovanadium organodiphosphonate family of materials suggested that the structural chemistry of these materials may be exceedingly complex[17] because the structural determinants may include the presence or absence of cations, the cation identity, and the tether length and additional functionality of the diphosphonate, as well as parameters of the hydrothermal reaction domain, such as the fill volume, pH, temperature, and presence of mineralizers such as HF.[18−23] To assess the structural consequences of some of these factors, we have reinvestigated the oxovanadium organodiphosphonate system, focusing on the influences of the absence or incorporation of organonitrogen cations and variations in the tether lengths of the diphosphonate ligands. Although the notoriously poor crystallinity of such materials renders their structural characterization difficult, we have succeeded in developing the structural chemistry of two classes of materials, the first consisting of charge-neutral V−P−O structures (types **1**−**3**) and the second based on anionic V−P−O substructures and incorporating organonitrogen cations (types **4**−**7**). The structures and properties of $[V_2O_2(H_2O)\{O_3P(CH_2)_nPO_3\}]\cdot xH_2O$ [$n = 2$, $x = 1$ (**1a**); $n = 3$, $x = 2$ (**1b**); $n = 4$, $x = 3$ (**1c**); $n = 5$, $x = 3$ (**1d**)], $[V_2O_2(H_2O)_4\{O_3P(CH_2)_6PO_3\}]$ (**2**), $[V_2O_2(H_2O)\{HO_3P(CH_2)_9PO_3H\}_2]$ (**3**), $[H_3N(CH_2)_nNH_3][V_4O_4(OH)_2\{O_3P(CH_2)_3PO_3\}_2]\cdot xH_2O$ [$n = 2$, $x = 6$ (**4a**); $n = 3$, $x = 3$ (**4b**); $n = 4$, $x = 2$ (**4c**); $n = 5$, $x = 1$ (**4d**); $n = 6$, $x = 0.5$ (**4e**); $n = 7$, $x = 0$ (**4f**)], and $[H_3NR]_y[V_4O_4(OH)_2\{O_3P(CH)_3PO_3\}_2]\cdot xH_2O$ [$R = -CH_2(NH_3)CH_2CH_3$, $y = 1$, $x = 0$ (**4g**); $R = -CH_3$, $n = 2$, $x = 3$ (**4h**); $R = -CH_2CH_3$, $y = 2$, $x = 1$ (**4i**); $R = -CH_2CH_2CH_3$, $y = 2$, $x = 0$ (**4j**); cation =

(5) Centi, G.; Trifiro, F.; Ebner, J. R.; Franchetti, V. M. *Chem. Rev.* **1988**, *88*, 55.
(6) Gleaves, J. T.; Centi, G. *Catal. Today* **1993**, *16*, 69.
(7) Sananes, M. T.; Hutchings, G. J.; Volta, J.-C. *J. Catal.* **1998**, *154*, 253.
(8) Hutchings, G. J. *J. Mater. Chem.* **2004**, *14*, 3385.
(9) Finn, R. C.; Zubieta, J.; Haushalter, R. C. *Prog. Inorg. Chem.* **2003**, *51*, 451.
(10) The chemistry of the metal organophosphonates has witnessed remarkable growth in the past decade. A number of useful reviews are available: (a) Vioux, A.; LeBideau, J.; Mutin, P. H.; Leclercq, D. *Top. Curr. Chem.* **2004**, *232*, 145. (b) Clearfield, A. *Curr. Opin. Solid State Mater. Sci.* **2003**, *6*, 495. (c) Clearfield, A. *Prog. Inorg. Chem.* **1998**, *47*, 371. (d) Alberti, G. In *Comprehensive Supramolecular Chemistry*; Atwood, J. L., Davis, J. E. D., Vogel, F., Eds.; Pergamon Press: New York, 1996; Vol. 9, p 152. (e) Clearfield, A. In *Comprehensive Supramolecular Chemistry*; Atwood, J. L., Davies, J. E. D., Vogel, F., Eds.; Pergamon Press: New York, 1996; Vol. 9, p 107. (f) Clearfield, A. *Chem. Mater.* **1998**, *10*, 2801. (g) Vermeulen, L. A. *Prog. Inorg. Chem.* **1997**, *44*, 143.
(11) Representative examples of recent work on metal organophosphonates include the following: (a) Kong, D.; Clearfield, A. *Chem. Commun.* **2005**, 1005. (b) Rao, K. P.; Balraj, V.; Minimol, M. P.; Vidyasagar, K. *Inorg. Chem.* **2004**, *43*, 4160 and references cited therein. (c) Gomez-Alcantara, M. M.; Cabya, A.; Martinez-Lara, M.; Arande, M. A. G.; Suau, R.; Bhuvanesh, N.; Clearfield, A. *Inorg. Chem.* **2004**, *43*, 5283. (d) Kong, D.; Li, Y.; Ouyang, X.; Prosvirin, A. V.; Zhao, H.; Ross, J. H.; Dunbar, K. R.; Clearfield, A. *Chem. Mater.* **2004**, *16*, 3020.
(12) Johnson, J. W.; Jacobson, A. J.; Butler, W. M.; Rosenthal, S. E.; Brody, J. F.; Lewandowski, J. T. *J. Am. Chem. Soc.* **1989**, *111*, 381.
(13) Huan, G.; Jacobson, A. J.; Johnson, J. W.; Corcoran, E. W. *Chem. Mater.* **1990**, *2*, 91.
(14) Zhu, J.; Bu, X.; Feng, P.; Stucky, G. D. *J. Am. Chem. Soc.* **2000**, *122*, 11563.
(15) Barton, T. J.; Bull, C. M.; Klemperer, W. G.; Loy, D. A.; McEnaney, B.; Misino, M.; Monson, P. A.; Pey, G.; Scherer, G. W.; Vartuli, J. C.; Yaghi, O. M. *Chem. Mater.* **1999**, *11*, 2633.
(16) Cheetham, A. K.; Ferey, G.; Loiseau, T. *Angew. Chem., Int. Ed.* **1999**, *38*, 3268.
(17) Soghomonian, V.; Chen, Q.; Haushalter, R. C.; Zubieta, J. *Angew. Chem., Int. Ed. Engl.* **1995**, *34*, 223.
(18) Soghomonian, V.; Diaz, R.; Haushalter, R. C.; O'Connor, C. J.; Zubieta, J. *Inorg. Chem.* **1995**, *34*, 4460.
(19) Soghomonian, V.; Haushalter, R. C.; Zubieta, J. *Chem. Mater.* **1995**, *7*, 1648.
(20) Bonavia, G.; Haushalter, R. C.; O'Connor, C. J.; Zubieta, J. *Inorg. Chem.* **1996**, *35*, 5603.
(21) Bonavia, G. H.; Haushalter, R. C.; Lu, S.; O'Connor, C. J.; Zubieta, J. *J. Solid State Chem.* **1997**, *132*, 144.
(22) Riou, D.; Serre, C.; Provost, J.; Ferey, G. *J. Solid State Chem.* **2000**, *155*, 238.
(23) Riou, D.; Baltazar, P.; Ferey, G. *Solid State Sci.* **2000**, *2*, 127.

$(H_2N(CH_2CH_3)_2)$, $y = 2$, $x = 0$ (**4k**)], $[H_3N(CH_2)_2NH_3][V_4O_4(OH)_2(H_2O)\{O_3P(CH_2)_5PO_3\}_2]\cdot H_2O$ (**5**), $[H_2N(CH_2CH_2)_2NH_2][V_2O_2\{O_3P(CH_2)_nPO_3H\}_2]$ [$n = 2$ (**6a**), $n = 4$ (**6b**), $n = 6$ (**6c**)], and $[H_3N(CH_2)_5NH_3][V_3O_3\{O_3P(CH_2)_2PO_3\}_2]$ (**7**) are described.

## Experimental Section

All chemicals were used as obtained without further purification. Vanadium(V) oxide, vanadyl sulfate hydrate, ammonium metavanadate, 1,2-diaminopropane, 1,3-diaminopropane, 1,4-diaminobutane, 1,5-diaminopentane, 1,6-diaminohexane, 1,7-diaminoheptane, piperazine, ethylenediamine, methylamine, ethylamine, propylamine, diethylamine, and hydrofluoric acid (48−51%) were purchased from Aldrich. The diphosphonate ligands 1,2-ethylenediphosphonic acid, 1,3-propylenediphosphonic acid, 1,4-butylenediphosphonic acid, 1,5-pentylenediphosphonic acid, 1,6-hexylenediphosphonic acid, and 1,9-nonylenediphosphonic acid were prepared according to the literature methods.[24,25] All syntheses were carried out in 23-mL poly(tetrafluoroethylene)-lined stainless steel containers under autogenous pressure. The reactants were stirred briefly, and the initial pH was measured before heating. Water was distilled above 3.0 MΩ in-house using a Barnstead model 525 Biopure Distilled Water Center. The initial and final pHs of the reactions were measured using Hydrion pH sticks.

**Synthesis of $[V_2O_2(H_2O)\{O_3P(CH_2)_2PO_3\}]\cdot H_2O$ (1a).** A solution of $V_2O_5$ (0.169 g, 0.929 mmol), 1,2-ethylenediphosphonic acid (0.178 g, 0.937 mmol), $H_2O$ (10.00 g, 556 mmol), and HF (0.200 mL, 5.80 mmol) with the mole ratio 0.99:1.00:593.4:6.19 was stirred briefly before heating to 200 °C for 72 h with initial and final pH values of 1.0 and 1.5, respectively. Dark-blue rods of **1a** were isolated in 90% yield and were suitable for X-ray diffraction. IR (KBr pellet, $cm^{-1}$): 3508(w), 3291(b), 1639(m), 1418(m), 1198(s), 1065(s), 1019(m), 939(s), 786(m).

**Synthesis of $[V_2O_2(H_2O)\{O_3P(CH_2)_3PO_3\}]\cdot 2H_2O$ (1b).** A solution of $VOSO_4$ (0.225 g, 1.380 mmol), 1,3-propylenediphosphonic acid (0.194 g, 0.937 mmol), $H_2O$ (10.00 g, 556 mmol), and HF (0.350 mL, 10.14 mmol) with the mole ratio 1.45:1.00:584.6:10.66 was stirred briefly before heating to 180 °C for 48 h with initial and final pH values of 1.5 and 1.5, respectively. Blue crystals of **1b** were isolated in 90% yield and were suitable for X-ray diffraction. IR (KBr pellet, $cm^{-1}$): 3515(w), 3227(b), 1630(m), 1410(m), 1178(s), 1065(s), 1025(m), 939(s), 786(m).

**Synthesis of $[V_2O_2(H_2O)\{O_3P(CH_2)_4PO_3\}]\cdot 3H_2O$ (1c).** A solution of $NH_4VO_3$ (0.107 g, 0.915 mmol), 1,4-butylenediphosphonic acid (0.210 g, 0.963 mmol), $H_2O$ (10.00 g, 556 mmol), and HF (0.300 mL, 8.70 mmol) with the mole ratio 0.95:1.00:577:9.0 was stirred briefly before heating to 200 °C for 96 h with initial and final pH values of 1.5 and 2.0, respectively. Blue plates of **1c** were isolated in 85% yield and were suitable for X-ray diffraction. IR (KBr pellet, $cm^{-1}$): 3553(b), 3219(b), 2930(w), 2858(w), 1634(m), 1454(m), 1404(m), 1332(m), 1296(w), 1169(s), 1070(s), 1020(m), 939(s), 786(m).

**Synthesis of $[V_2O_2(H_2O)\{O_3P(CH_2)_5PO_3\}]\cdot 3H_2O$ (1d).** A solution of $NH_4VO_3$ (0.107 g, 0.915 mmol), 1,5-pentylenediphosphonic acid (0.220 g, 0.948 mmol), $H_2O$ (10.00 g, 556 mmol), and HF (0.300 mL, 8.70 mmol) with the mole ratio 0.97:1.00:587:9.18 was stirred briefly before heating to 200 °C for 96 h with initial and final pH values of 1.5 and 1.5, respectively. Blue crystals of **1d** were isolated in 85% yield and were suitable for X-ray diffraction. IR (KBr pellet, $cm^{-1}$): 3553(b), 3201(b), 2939(w), 2867(w), 1634(m), 1458(m), 1404(m), 1314(m), 1169(s), 1076(s), 1020(m), 944(s), 790(m).

**Synthesis of $[V_2O_2(H_2O)_4\{O_3P(CH_2)_6PO_3\}]$ (2).** A solution of $NH_4VO_3$ (0.107 g, 0.915 mmol), 1,6-hexylenediphosphonic acid (0.231 g, 0.939 mmol), $H_2O$ (5.00 g, 278 mmol), and HF (0.300 mL, 8.70 mmol) with the mole ratio 0.97:1.00:296:9.27 was stirred briefly before heating to 180 °C for 96 h with initial and final pH values of 1.5 and 1.5, respectively. Blue rods of **2** were isolated in 5% yield and were suitable for X-ray diffraction. IR (KBr pellet, $cm^{-1}$): 3445(m), 2939(w), 2849(w), 1553(m), 1539(w), 1503(w), 1454(w), 1183(w), 1106(m), 1083(m), 1029(s), 1007(m), 984(m), 921(w), 700(m).

**Synthesis of $[VO\{HO_3P(CH_2)_9PO_3H\}]$ (3).** A solution of $NH_4VO_3$ (0.088 g, 0.752 mmol), 1,9-nonylenediphosphonic acid (0.221 g, 0.767 mmol), $H_2O$ (10.00 g, 556 mmol), and HF (0.200 mL, 5.80 mmol) with the mole ratio 0.98:1.00:725:7.60 was stirred briefly before heating to 180 °C for 96 h with initial and final pH values of 1.5 and 2.0, respectively. Blue crystals of **3** were isolated in 25% yield and were suitable for X-ray diffraction. IR (KBr pellet, $cm^{-1}$): 3445(s), 2930(m), 2849(m), 1467(m), 1395(w), 1129(s), 1047(s), 980(m), 908(m), 795(m), 722(w).

**Synthesis of $[NH_3(CH_2)_2NH_3][V_4O_4(OH)_2(H_2O)_2\{O_3P(CH_2)_3PO_3\}_2]\cdot 4H_2O$ (4a).** A mixture of $V_2O_5$ (0.169 g, 0.929 mmol), 1,3-propylenediphosphonic acid (0.191 g, 0.936 mmol), $H_2O$ (10.00 g, 556 mmol), ethylenediamine (0.085 mL, 1.27 mmol), and HF (0.250 mL, 7.25 mmol) in the mole ratio 1.00:1.00:599:1.18:7.80 was stirred briefly before heating to 200 °C for 72 h. Initial and final pH values of 2.5 and 2.5, respectively, were recorded. Blue crystals of **4a** suitable for X-ray diffraction were isolated in 90% yield. IR (KBr pellet, $cm^{-1}$): 3499(s), 3120(m), 2948(w), 1634(m), 1553(w), 1413(w), 1354(w), 1201(m), 1156(m), 1020(s), 980(m), 908(m), 772(m), 722(w).

**Synthesis of $[NH_3(CH_2)_3NH_3][V_4O_4(OH)_2\{O_3P(CH_2)_3PO_3\}_2]\cdot 3H_2O$ (4b).** A mixture of $V_2O_5$ (0.169 g, 0.929 mmol), 1,3-propylenediphosphonic acid (0.191 g, 0.936 mmol), $H_2O$ (10.00 g, 556 mmol), 1,3-diaminopropane (0.092 mL, 1.10 mmol), and HF (0.250 mL, 7.25 mmol) in the mole ratio 1.00:1.00:599:1.18:7.80 was stirred briefly before heating to 200 °C for 72 h. Initial and final pH values of 2.5 and 2.5, respectively, were recorded. Blue crystals of **4b** suitable for X-ray diffraction were isolated in 90% yield. IR (KBr pellet, $cm^{-1}$): 3499(s), 3120(m), 2948(w), 1634(m), 1553(w), 1413(w), 1354(w), 1201(m), 1156(m), 1020(s), 980(m), 908(m), 772(m), 722(w).

**Synthesis of $[H_3N(CH_2)_4NH_3][V_4O_4(OH)_2\{O_3P(CH_2)_3PO_3\}_2]\cdot 2.5H_2O$ (4c).** A solution of $V_2O_5$ (0.170 g, 0.935 mmol), 1,3-propylenediphosphonic acid (0.191 g, 0.936 mmol), $H_2O$ (10.00 g, 556 mmol), 1,4-diaminobutane (0.100 g, 1.13 mmol), and HF (0.150 mL, 4.35 mmol) in the mole ratio 1.00:1.00:594:0.96:4.60 was stirred briefly before heating to 200 °C for 72 h (initial and final pH values were 2.5 and 3.0, respectively). Blue crystals of **4c** suitable for X-ray diffraction were isolated in 90% yield. IR (KBr pellet, $cm^{-1}$): 3508(s), 3101(m), 2957(w), 1630(m), 1503(m), 1458(w), 1413(w), 1354(w), 1196(m), 1147(m), 1020(s), 980(m), 772(m), 718(w).

**Synthesis of $[H_3N(CH_2)_5NH_3][V_4O_4(OH)_2\{O_3P(CH_2)_3PO_3\}_2]\cdot H_2O$ (4d).** A solution of $V_2O_5$ (0.170 g, 0.935 mmol), 1,3-propylenediphosphonic acid (0.191 g, 0.936 mmol), $H_2O$ (10.00 g, 556 mmol), 1,5-diaminopentane (0.105 mL, 0.897 mmol), and HF (0.150 mL, 4.35 mmol) in the mole ratio 1.00:1.00:594:0.96:4.60 was stirred briefly before heating to 200 °C for 72 h (the initial and final pH values were 2.5 and 3.0, respectively). Blue crystals of **4d** suitable for X-ray diffraction were isolated in 90% yield. IR

(24) Arnold. D. I.; Ouyang, X.; Clearfield, A. *Chem. Mater.* **2002**, *14*, 2020.
(25) Horne, J. C.; Blanchard, C. J. *J. Am. Chem. Soc.* **1996**, *118*, 12788.

(KBr pellet, $cm^{-1}$): 3508(s), 3101(m), 2957(w), 1630(m), 1503(m), 1458(w), 1413(w), 1354(w), 1196(m), 1147(m), 1020(s), 980(m), 772(m), 718(w).

**Synthesis of $[H_3N(CH_2)_6NH_3][V_4O_4(OH)_2\{O_3P(CH_2)_3PO_3\}_2]\cdot 0.5H_2O$ (4e).** A solution of $V_2O_5$ (0.170 g, 0.935 mmol), 1,3-propylenediphosphonic acid (0.190 g, 0.931 mmol), $H_2O$ (10.00 g, 556 mmol), 1,6-diaminohexane (0.115 g, 0.986 mmol), and HF (0.200 mL, 5.80 mmol) in the mole ratio 1.00:1.00:597:1.18:6.20 was heated at 200 °C for 72 h (initial and final pH values were 2.0 and 2.5, respectively). Blue plates of **4e** were isolated in 90% yield. IR (KBr pellet, $cm^{-1}$): 3535(s), 3083(w), 1634(m), 1530(m), 1463(w), 1413(w), 1350(w), 1255(w), 1201(m), 1142(m), 1020(s), 980(m), 772(m), 718(m).

**Synthesis of $[H_3N(CH_2)_7NH_3][V_4O_4(OH)_2\{O_3P(CH_2)_3PO_3\}_2]$ (4f).** A solution of $V_2O_5$ (0.170 g, 0.935 mmol), 1,3-propylenediphosphonic acid (0.191 g, 0.936 mmol), $H_2O$ (10.00 g, 556 mmol), 1.7-diaminoheptane (0.115 g, 0.884 mmol), and HF (0.150 mL, 4.35 mmol) in the mole ratio 1.00:1.00:594:0.96:4.60 was stirred briefly before heating to 200 °C for 72 h (initial and final pH values were 2.5 and 3.0, respectively). Blue crystals of **4f** suitable for X-ray diffraction were isolated in 90% yield. IR (KBr pellet, $cm^{-1}$): 3508(s), 3101(m), 2957(w), 1630(m), 1503(m), 1458(w), 1413(w), 1354(w), 1196(m), 1147(m), 1020(s), 980(m), 772(m), 718(w).

**Synthesis of $[CH_3CH_2(NH_3)CH_2NH_3][V_4O_4(OH)_2\{O_3P(CH_2)_3PO_3\}_2]$ (4g).** A solution of $V_2O_5$ (0.170 g, 0.935 mmol), 1,3-propylenediphosphonic acid (0.190 g, 0.931 mmol), $H_2O$ (10.00 g, 556 mmol), 1,2-diaminopropane (0.092 mL, 1.10 mmol), and HF (0.200 mL, 5.80 mmol) in the mole ratio 1.00:1.00:597:1.18:6.20 was heated at 200 °C for 72 h (initial and final pH values of 2.0 and 2.5, respectively). Blue plates of **4g** were isolated in 45% yield. IR (KBr pellet, $cm^{-1}$): 3535(s), 3083(w), 1634(m), 1530(m), 1463(w), 1413(w), 1350(w), 1255(w), 1201(m), 1142(m), 1020(s), 980(m), 772(m), 718(m).

**Synthesis of $[NH_3CH_3]_2[V_4O_4(OH)_2\{O_3P(CH_2)_3PO_3\}_2]\cdot 3H_2O$ (4h).** A mixture of $V_2O_5$ (0.169 g, 0.929 mmol), 1,3-propylenediphosphonic acid (0.191 g, 0.936 mmol), $H_2O$ (10.00 g, 556 mmol), methylamine (40%; 0.310 mL, 3.99 mmol), and HF (0.100 mL, 2.90 mmol) in the mole ratio 1.00:1.00:599:4.26:3.10 was stirred briefly before heating to 200 °C for 48 h. Initial and final pH values of 3.5 and 3.5, respectively, were recorded. Blue plates of **4h** suitable for X-ray diffraction were isolated in 90% yield. IR (KBr pellet, $cm^{-1}$): 3499(s), 3120(m), 2948(w), 1634(m), 1553(w), 1413(w), 1354(w), 1201(m), 1156(m), 1020(s), 980(m), 908(m), 772(m), 722(w).

**Synthesis of $[NH_3CH_2CH_3]_2[V_4O_4(OH)_2\{O_3P(CH_2)_3PO_3\}_2]\cdot H_2O$ (4i).** A solution of $V_2O_5$ (0.170 g, 0.935 mmol), 1,3-propylenediphosphonic acid (0.191 g, 0.936 mmol), $H_2O$ (10.00 g, 556 mmol), ethylamine (70%) (0.250 mL, 3.88 mmol), and HF (0.050 mL, 1.45 mmol) in the mole ratio 1:00:1.00:594:4.14:1.55 was stirred briefly before heating to 200 °C for 48 h (initial and final pH values were 3.0 and 4.5, respectively). Blue plates of **4i** suitable for X-ray diffraction were isolated in 90% yield. IR (KBr pellet, $cm^{-1}$): 3508(s), 3101(m), 2957(w), 1630(m), 1503(m), 1458(w), 1413(w), 1354(w), 1196(m), 1147(m), 1020(s), 980(m), 772(m), 718(w).

**Synthesis of $[NH_3CH_2CH_2CH_3]_2[V_4O_4(OH)_2\{O_3P(CH_2)_3PO_3\}_2]$ (4j).** A solution of $V_2O_5$ (0.170 g, 0.935 mmol), 1,3-propylenediphosphonic acid (0.190 g, 0.931 mmol), $H_2O$ (10.00 g, 556 mmol), propylamine (0.220 mL, 3.72 mmol), and HF (0.050 mL, 1.45 mmol) in the mole ratio 1.00:1.00:597:3.97:1.55 was heated at 200 °C for 48 h (initial and final pH values of 3.0 and 4.0, respectively). Blue rods of **4j** were isolated in 85% yield. IR (KBr pellet, $cm^{-1}$): 3535(s), 3083(w), 1634(m), 1530(m), 1463(w), 1413(w), 1350(w), 1255(w), 1201(m), 1142(m), 1020(s), 980(m), 772(m), 718(m).

**Synthesis of $[NH_2(CH_2CH_3)_2]_2[V_4O_4(OH)_2\{O_3P(CH_2)_3PO_3\}_2]\cdot 4H_2O$ (4k).** A mixture of $V_2O_5$ (0.169 g, 0.929 mmol), 1,3-propylenediphosphonic acid (0.191 g, 0.936 mmol), $H_2O$ (10.00 g, 556 mmol), diethylamine (0.270 mL, 2.46 mmol), and HF (0.075 mL, 2.18 mmol) in the mole ratio 1.00:1.00:599:2.63:2.33 was stirred briefly before heating to 200 °C for 48 h. Initial and final pH values of 4.0 and 4.5, respectively, were recorded. Blue rods of **4k** suitable for X-ray diffraction were isolated in 70% yield. IR (KBr pellet, $cm^{-1}$): 3499(s), 3120(m), 2948(w), 1634(m), 1553(w), 1413(w), 1354(w), 1201(m), 1156(m), 1020(s), 980(m), 908(m), 772(m), 722(w).

**Synthesis of $[H_3N(CH_2)_2NH_3][V_4O_4(OH)_2\{O_3P(CH_2)_5PO_3\}_2]\cdot 0.75H_2O$ (5).** A solution of $NH_4VO_3$ (0.219 g, 1.872 mmol), 1,5-pentylenediphosphonic acid (0.218 g, 0.939 mmol), $H_2O$ (10.00 g, 556 mmol), ethylenediamine (0.090 mL, 1.34 mmol), and HF (0.200 mL, 5.80 mmol) in the mole ratio 2.00:1.00:593:1.43:6.20 was heated at 180 °C for 72 h (initial and final pH values of 3.0 and 3.5, respectively). Blue plates of **5** suitable for X-ray diffraction were isolated in 75% yield. IR (KBr pellet, $cm^{-1}$): 3454(s), 3218(w), 3038(m), 2930(m), 1621(m), 1508(m), 1454(w), 1408(w), 1300(w), 1038(s), 980(m), 799(m), 709(w).

**Synthesis of $[NH_2(CH_2CH_2)_2NH_2][V_2O_2\{HO_3P(CH_2)_2PO_3\}_2]$ (6a).** A solution of $V_2O_5$ (0.169 g, 0.929 mmol), 1,2-ethylenediphosphonic acid (0.180 g, 0.947 mmol), $H_2O$ (10.00 g, 556 mmol), piperazine (0.122 g, 1.42 mmol), and HF (0.250 mL, 7.25 mmol) in the mole ratio 0.98:1.00:587:1.50:7.66 was heated to 200 °C for 72 h to provide blue plates of **6a** in 85% yield (initial pH, 2.0; final pH, 2.5). IR (KBr pellet, $cm^{-1}$): 3047(m), 2921(w), 2822(w), 2560(w), 2488(w), 1621(m), 1454(m), 1413(w), 1323(w), 1196(m), 1142(m), 1043(s), 939(m), 871(w), 772(m), 709(m).

**Synthesis of $[NH_2(CH_2CH_2)_2NH_2][V_2O_2\{HO_3P(CH_2)_4PO_3\}_2]$ (6b).** The reaction of $V_2O_5$ (0.133 g, 0.731 mmol), 1,4-butylenediphosphonic acid (0.083 g, 0.381 mmol), $H_2O$ (10.00 g, 556 mmol), piperazine (0.101 g, 1.17 mmol), and HF (0.250 mL, 5.80 mmol) in the mole ratio 1.92:1.00:1459:3.08:15.2 at 180 °C for 96 h produced blue plates of **6b** in 65% yield (initial pH, 3.0; final pH, 3.0). IR (KBr pellet, $cm^{-1}$): 3056(m), 2948(w), 2731(w), 2560(w), 2488(w), 2361(w), 1616(m), 1458(m), 1408(w), 1323(w), 1192(w), 1143(w), 1043(s), 1007(m), 957(m), 935(m), 777(m), 709(m).

**Synthesis of $[NH_2(CH_2CH_2)_2NH_2][V_2O_2\{HO_3P(CH_2)_6PO_3\}]$ (6c).** A solution of $V_2O_5$ (0.134 g, 0.737 mmol), 1,6-hexylenediphosphonic acid (0.096 g, 0.390 mmol), $H_2O$ (10.00 g, 556 mmol), piperazine (0.101 g, 1.17 mmol), and HF (0.200 mL, 5.80 mmol) in the mole ratio 1.89:1.00:1426:3.00:14.87 was stirred briefly before heating to 180 °C for 72 h. The initial and final pH values were 2.5 and 2.5, respectively. Blue rods of **6c** suitable for X-ray diffraction were isolated in 75% yield. IR (KBr pellet, $cm^{-1}$): 3047(m), 2939(w), 2849(w), 2560(w), 2479(w), 1612(w), 1458(m), 1408(w), 1327(w), 1183(w), 1151(m), 1043(s), 1011(m), 944(m), 804(w), 777(m), 754(m), 713(m).

**Synthesis of $[H_3N(CH_2)_5NH_3][(V_3O_3)\{O_3P(CH_2)_2PO_3\}_2]$ (7).** A mixture of $V_2O_5$ (0.170 g, 0.935 mmol), 1,2-ethylenediphosphonic acid (0.175 g, 0.921 mmol), $H_2O$ (5.00 g, 278 mmol), 1,5-diaminopentane (0.125 mL, 0.539 mmol), and HF (0.350 mL, 10.14 mmol) in the mole ratio 1.00:1.00:302:0.59:11.0 was heated to 180 °C for 48 h. Initial and final pH values of 1.5 and 2.0, respectively, were recorded. Green crystals of **7** suitable for X-ray diffraction were isolated in 90% yield. IR (KBr pellet, $cm^{-1}$): 3138(m), 3065-

(m), 2930(w), 2849(w), 1601(m), 1509(m), 1467(w), 1408(w), 1295(m), 1177(m), 1086(s), 1048(s), 1000(m), 993(s), 813(w), 738-(m).

**X-ray Crystallography.** Crystallographic data for the compounds were collected with a Bruker P4 diffractometer equipped with a SMART CCD system[26] and using Mo Kα radiation ($\lambda$ = 0.710 73 Å). The data were collected at 90 K and corrected for Lorentz and polarization effects.[27] Absorption corrections were made using *SADABS*.[28] The structure solutions and refinements were carried out using the *SHELXTL*[29] crystallographic software package. The structures were solved using direct methods, and non-hydrogen atoms were located from the initial solution. After locating all of the non-hydrogen atoms in each structure, the model was refined against $F^2$, initially using isotropic and then anisotropic thermal displacement parameters, until the final value of $\Delta/\sigma_{max}$ was less than 0.001. Hydrogen atoms were introduced in calculated positions and refined isotropically. Neutral atom-scattering coefficients and anomalous dispersion corrections were taken from the *International Tables*, Vol. C.

For compound **3**, the V1 and V2 sites are disordered about two positions along the O4−V1−O5−V2−O6 vector. The vanadium sites occupy positions above and below the O4 plane of the diphosphonate oxygen donors so as to produce the long−short V−O bond length alternations {O4═V1a−O5═V2b−O6} and {O4−V1b═O5−V2b═O6}. This behavior is quite common in vanadium oxide phases.[20] The V1 site of compound **4g** is also disordered along the V1−O2 vector. The $[H_3NCH_2CH(NH_3)CH_3]^{2+}$ cation of **4g** is disordered about the center of symmetry at 0.25, 0.25, 0.

**4h** was determined to be a nonmerohedral twin from the initial diffraction pattern. The program *Cell_Now*[30] was used to determine that **4h** was composed of two crystal domains, with the second domain rotated by 180° with respect to the first crystal domain. A twin law was created and imported into the *SAINT-Plus* software package,[31] where the data were corrected for Lorentz and polarization effects and absorption using *TWINABS*.[32] The structure was then solved by direct methods.

Crystallographic details have been summarized in Table 1. Selected bond lengths and angles for the structures are summarized in Table 2.

**Magnetism.** The magnetic data were recorded on polycrystalline samples of **1** in the 2−300 K temperature range using a Quantum Design MPMS-5S SQUID spectrometer. Calibrating and operating procedures have been reported elsewhere.[33] The temperature-dependent magnetic data were obtained at a magnetic field of $H$ = 1000 Oe.

**Thermogravimetric Analysis (TGA).** TGA studies were performed using 10−25-mg samples in a TA Instruments TGA Q 500 under a 50 mL/min flow of synthetic air. The temperature was ramped from 25 to 650 °C at a rate of 5 °C/min for the decomposition.

**Thermodiffraction.** Thermodiffraction data were collected on a Bruker AXS D8 Advance automated diffractometer equipped with a TTK 450 heating stage using Cu Kα radiation. The powder was placed in the sample holder, which acted as the heating system. The step size was 0.02° in 2$\theta$, and the heating rate from room temperature to 275 °C was 0.5 °C/s and that for the temperature range from 300 to 425 °C was 0.2 °C/s. The delay time between reaching the set temperature and measuring the diffraction pattern was 5 min. All temperature spectra were collected under vacuum.

## Results and Discusson.

**Syntheses and IR Spectroscopy.** The metal−oxide hybrids of this study were prepared by conventional hydrothermal methods,[34−40] which are now routinely applied to the isolation of organic−inorganic composite materials.[41] The materials of the oxovanadium organodiphosphonate family (types **1**−**3**) were prepared from a vanadate salt, the appropriate diphosphonate, and $H_2O$ in the presence of a small amount of HF, acting as a mineralizer. In the absence of HF, only microcrystalline materials could be isolated. HF presumably modifies the solubility of the reactants and products and promotes crystal growth. The compounds of the oxovanadium organodiphosphonate-organoammonium cation class (types **4**−**7**) were similarly synthesized from the appropriate vanadium source, a diphosphonate, an organonitrogen compound, and water at 180−200 °C for 72−96 h, in the presence of HF.

Crystals suitable for single-crystal X-ray studies were obtained for oxides of types **1**−**3** for diphosphonates $\{O_3P(CH_2)_nPO_3\}^{4-}$ with $n$ = 2−6 and 9. Microcrystalline materials were obtained for $n$ = 7, 8, 10, and 12, and those with $n$ = 7 and 8 were isomorphous with **2** while those with $n$ = 10 and 12 were isomorphous with **3**. For the materials with entrained organoammonium cations (types **4**−**7**) suitable crystalline materials were obtained for $n$ = 2−6. For $n \geq 7$, only mixtures were observed under the conditions of synthesis.

The IR spectra of all materials exhibit a band in the 945−983-$cm^{-1}$ region assigned to $\nu$(V═O). A series of three or four bands in the 1000−1200-$cm^{-1}$ region is characteristic of the ($RPO_3$) group.[42] The O−H stretching bands of the water of crystallization are observed at ca. 3200 $cm^{-1}$. The band is absent in the IR spectra of **2**, **3**, **4f**, **4g**, **6a**−**c**, and **7**, which do not contain any water molecules. The broad bands observed in all cases at 2800−2950 $cm^{-1}$ are most likely associated with strongly hydrogen-bonded hydroxyl groups or coordinated water molecules.[43]

**X-ray Structures.** The common structural motif of inorganic layers, V−P−O in these cases, buttressed by the


(26) *SMART, Data Collection Software*, version 5.630; Bruker-AXS Inc.: Madison, WI, 1997−2002.
(27) *SAINT Plus, Data Reduction Software*, version 6.45A; Bruker-AXS Inc.: Madison, WI, 1997−2002.
(28) Sheldrick, G. M. *SADABS*; University of Göttingen: Göttingen, Germany, 1996.
(29) *SHELXTL PC*, version 6.12; Bruker-AXS Inc.: Madison, WI, 2002.
(30) Sheldrick, G. M. *Cell-Now*, 1-22-2004; Bruker-AXS Inc.: Göttingen, Germany, 2004.
(31) Sheldrick, G. M. *SAINT-Plus*, Versionn 6.45; Bruker-AXS Inc.: Madison, WI, 1996.
(32) Sheldrick, G. M. *TWINABS: Program for the Empirical Absorption Corrections for Twins*; Bruker-AXS Inc.: Madison, WI, 2003.
(33) O'Connor, C. J. *Prog. Inorg. Chem.* **1979**, *29*, 203.
(34) Whittingham, M. S. *Curr. Opin. Solid State Mater. Sci.* **1996**, *1*, 227.
(35) Gopalakrishnan, J. *Chem. Mater.* **1995**, *7*, 1265.
(36) Fing, S.; Xu, R. *Acc. Chem. Res.* **2001**, *34* 239.
(37) Rabenau, A. *Angew. Chem., Int. Ed. Engl.* **1985**, *24*, 1026.
(38) Weller, M.; Dann, S. E. *Curr. Opin. Solid State Mater. Sci.* **1998**, *3*, 137.
(39) Laudise, P. A. *Chem. Eng. News* **1987**, Sept 28, 30−43.
(40) Stein, A.; Keller, S. W.; Mallouk, T. E. *Science* **1993**, *289*, 1558.
(41) Zubieta, J. *Compr. Coord. Chem. II* **2004**, *1*, 697.
(42) Ortiz-Avila, C. Y.; Bhardraj, C.; Clearfield, A. *Inorg. Chem.* **1994**, *33*, 2499.
(43) Poojary, D. M.; Zhang, B.; Bellinghausen, P.; Clearfield, A. *Inorg. Chem.* **1996**, *35*, 4942.

**Table 1.** Crystal Data for the Structures of $[V_2O_2(H_2O)\{O_3P(CH_2)_nPO_3\}]\cdot xH_2O$ [$n = 2$, $x = 1$ (**1a**); $n = 3$, $x = 2$ (**1b**); $n = 4$, $x = 3$ (**1c**); $n = 5$, $x = 3$ (**1d**)], $[V_2O_2(H_2O)_4\{O_3P(CH_2)_6PO_3\}]$ (**2**), $[V_2O_2(H_2O)\{HO_3P(CH_2)_9PO_3H\}_2]$ (**3**), (cat.)$[V_4O_6(OH)_2\{O_3P(CH_2)_3PO_3\}_2]\cdot xH_2O$ [cat. = $\{H_3N(CH_2)_2NH_3\}^{2+}$, $x = 4$ (**4a**); cat. = $\{H_3N(CH_2)_3NH_3\}^{2+}$, $x = 3$ (**4b**); cat. = $\{H_3N(CH_2)_4NH_3\}^{2+}$, $x = 2$ (**4c**); cat. = $\{H_3N(CH_2)_5NH_3\}^{2+}$, $x = 1$ (**4d**); cat. = $\{H_3N(CH_2)_6NH_3\}^{2+}$, $x = 0.5$ (**4e**); cat. = $\{H_3N(CH_2)_7NH_3\}^{2+}$, $x = 0$ (**4f**); cat. = $\{CH_3CH_2(NH_3)CH_2NH_3)\}^{2+}$, $x = 0$ (**4g**); cat. = $2x\{NH_3CH_3\}^{+}$, $x = 3.0$ (**4h**); cat. = $2x\{NH_3CH_2CH_3\}^{+}$, $x = H_2O$ (**4i**); cat. = $2x\{NH_3CH_2CH_2CH_3\}^{+}$, $x = 0$ (**4j**); cat. = $2x\{NH_2(CH_2CH_3)_2\}^{+}$, $x = 4H_2O$ (**4k**)] $[H_3N(CH_2)_2NH_3][V_4O_4(OH)_2\{H_2O\}\{O_3P(CH_2)_5PO_3\}_2]\cdot H_2O$ (**5**), $[H_2N(CH_2CH_2)_2NH_2][V_2O_2\{O_3P(CH_2)_nPO_3H\}_2]$ [$n = 2$ (**6a**), $n = 4$ (**6b**), $n = 6$ (**6c**)], and $[H_3N(CH_2)_5NH_3][V_3O_3\{O_3P(CH_2)_2PO_3\}_2]$ (**7**)

| | **1a** | **1b** | **1c** | **1d** | **2** | **3** |
|---|---|---|---|---|---|---|
| empirical formula | $C_{0.5}H_2O_{2.5}P_{0.5}V_{0.5}$ | $C_{0.75}H_3O_{2.75}P_{0.5}V_{0.5}$ | $C_1H_4O_3P_{0.5}V_{0.5}$ | $C_{1.25}H_{4.5}O_3P_{0.5}V_{0.5}$ | $C_3H_{10}O_6PV$ | $C_{4.5}H_{10}O_{3.5}PV_{0.5}$ |
| fw | 88.98 | 96.99 | 105.00 | 108.50 | 224.02 | 176.57 |
| cryst syst | orthorhombic | orthorhombic | orthorhombic | orthorhombic | monoclinic | tetragonal |
| space group | *Cmcm* | *Immm* | *Cmcm* | *Immm* | $P2_1/c$ | $I4/m$ |
| *a*, Å | 7.4670(5) | 7.427(1) | 7.4362(5) | 7.4330(4) | 14.094(1) | 8.9297(3) |
| *b*, Å | 13.8824(9) | 9.348(2) | 19.149(1) | 9.3673(5) | 5.2746(4) | |
| *c*, Å | 9.3289(6) | 16.793(3) | 9.3446(6) | 21.836(1) | 10.1660(8) | 34.847(2) |
| $\beta$, deg | | | | | 94.606(2) | |
| *V*, Å$^3$ | 967.0(1) | 1165.8(3) | 1330.6(2) | 1520.4(1) | 753.3(1) | 2778.6 |
| *Z* | 16 | 16 | 16 | 16 | 4 | 16 |
| $D_{calc}$, g cm$^{-3}$ | 2.445 | 2.430 | 2.096 | 1.896 | 1.975 | 1.688 |
| $\mu$, mm$^{-1}$ | 2.305 | 2.210 | 1.703 | 1.494 | 1.511 | 0.968 |
| *T*, K | 90 | 90 | 90 | 90 | 90 | 90 |
| $\lambda$, Å | 0.71073 | 0.71073 | 0.71073 | 0.71073 | 0.71073 | 0.71073 |
| R1 | 0.0233 | 0.0578 | 0.0435 | 0.0408 | 0.0601 | 0.0290 |
| wR2 | 0.0715 | 0.1217 | 0.0789 | 0.0948 | 0.1149 | 0.0744 |

| | **4a** | **4b** | **4c** | **4d** | **4e** | **4f** |
|---|---|---|---|---|---|---|
| empirical formula | $C_4H_{17.5}NO_{11.75}P_2V_2$ | $C_{4.5}H_{16}NO_{10.5}P_2V_2$ | $C_5H_{16.5}NO_{10.25}P_2V_2$ | $C_{5.5}H_{16}O_{9.5}NP_2V_2$ | $C_6H_{16.5}NO_{9.25}P_2V_2$ | $C_{6.5}H_{17}NO_9P_2V_2$ |
| fw | 431.51 | 416.00 | 418.51 | 412.01 | 414.52 | 417.03 |
| cryst syst | monoclinic | monoclinic | monoclinic | monoclinic | monoclinic | monoclinic |
| space group | *C*2/*c* | *C*2/*c* | *C*2/*c* | *C*2/*c* | *C*2/*c* | *C*2/*c* |
| *a*, Å | 14.579(1) | 15.5527(7) | 15.200(1) | 15.712(1) | 15.640(1) | 15.822(2) |
| *b*, Å | 10.2424(8) | 10.0841(5) | 10.2122(7) | 10.030(1) | 10.2112(7) | 10.0614(9) |
| *c*, Å | 18.782(1) | 18.7813(8) | 18.590(1) | 18.656(2) | 18.6795(14) | 18.610(2) |
| $\beta$, deg | 98.837(1) | 104.423(1) | 103.530(1) | 103.328(2) | 105.484(1) | 104.292(2) |
| *V*, Å$^3$ | 2771.3(4) | 2852.7 | 2805.7(3) | 2861.0(5) | 2875.0(4) | 2870.9(5) |
| *Z* | 8 | 8 | 8 | 8 | 8 | 8 |
| $D_{calc}$, g cm$^{-3}$ | 2.068 | 1.937 | 1.982 | 1.913 | 1.915 | 1.930 |
| $\mu$, mm$^{-1}$ | 1.639 | 1.582 | 1.608 | 1.572 | 1.564 | 1.565 |
| *T*, K | 90 | 90 | 90 | 90 | 90 | 90 |
| $\lambda$, Å | 0.71073 | 0.71073 | 0.71073 | 0.71073 | 0.71073 | 0.71073 |
| R1 | 0.0456 | 0.0331 | 0.0597 | 0.0445 | 0.0669 | 0.0627 |
| wR2 | 0.1115 | 0.0826 | 0.1382 | 0.1014 | 0.1498 | 0.1184 |

| | **4g** | **4h** | **4i** | **4j** | **4k** | **5** |
|---|---|---|---|---|---|---|
| empirical formula | $C_{4.5}H_{12.75}NO_9P_2V_2$ | $C_4H_{16}NO_{10.50}P_2V_2$ | $C_5H_{15}NO_{9.50}P_2V_2$ | $C_6H_{17}NO_9P_2V_2$ | $C_7H_{19.50}NO_9P_2V_2$ | $C_{12}H_{32.75}N_2O_{18.75}P_4V_4$ |
| fw | 388.73 | 410.00 | 405.00 | 411.03 | 425.56 | 832.79 |
| cryst syst | monoclinic | monoclinic | monoclinic | monoclinic | monoclinic | orthorhombic |
| space group | *C*2/*c* | *C*2/*c* | *C*2/*c* | *C*2/*c* | *C*2/*c* | $Cmc2_1$ |
| *a*, Å | 15.235(1) | 15.003(3) | 15.0877(9) | 15.4228(9) | 15.2768(8) | 30.947(2) |
| *b*, Å | 10.1817(6) | 10.126(2) | 10.2027(6) | 10.2047(6) | 10.2216(6) | 10.6168(8) |
| *c*, Å | 18.697(1) | 18.604(4) | 18.6376(11) | 18.7078(11) | 18.6279(10) | 18.604(1) |
| $\beta$, deg | 103.524(1) | 101.00(3) | 102.5210(10) | 103.8350(10) | 103.2520(10) | |
| *V*, Å$^3$ | 2819.7(3) | 2774.3(10) | 2800.7(3) | 2858.9(3) | 2831.4(3) | 6112.5(8) |
| *Z* | 8 | 8 | 8 | 8 | 8 | 8 |
| $D_{calc}$, g cm$^{-3}$ | 1.831 | 1.963 | 1.921 | 1.910 | 1.997 | 1.810 |
| $\mu$, mm$^{-1}$ | 1.586 | 1.625 | 1.604 | 1.570 | 1.589 | 1.472 |
| *T*, K | 90 | 90 | 90 | 90 | 90 | 90 |
| $\lambda$, Å | 0.71073 | 0.71073 | 0.71073 | 0.71073 | 0.71073 | 0.71073 |
| R1 | 0.0604 | 0.0803 | 0.0442 | 0.0367 | 0.0529 | 0.0705 |
| wR2 | 0.1210 | 0.1654 | 0.1114 | 0.0964 | 0.1461 | 0.1331 |

| | **6a** | **6b** | **6c** | **7** |
|---|---|---|---|---|
| empirical formula | $C_4H_{11}NO_7P_2V$ | $C_6H_{15}NO_7P_2V$ | $C_8H_{19}NO_7P_2V$ | $C_9H_{24}N_2O_{15}P_4V_3$ |
| fw | 298.02 | 326.07 | 354.12 | 677.00 |
| cryst syst | monoclinic | monoclinic | monoclinic | monoclinic |
| space group | $P2_1/c$ | $P2_1/c$ | $P2_1/c$ | $P2_1/c$ |
| *a*, Å | 12.2895(15) | 14.605(1) | 16.941(3) | 16.325(2) |
| *b*, Å | 13.466(2) | 13.4811(9) | 13.470(2) | 13.336(1) |
| *c*, Å | 6.0846(7) | 6.0678(4) | 6.055(1) | 10.1019(9) |
| $\beta$, deg | 103.401(2) | 98.730(1) | 95.026(4) | 89.994(2) |
| *V*, Å$^3$ | 979.5(2) | 1180.8(1) | 1376.5(4) | 2199.3(3) |
| *Z* | 4 | 4 | 4 | 4 |
| $D_{calc}$, g cm$^{-3}$ | 2.021 | 1.834 | 1.709 | 2.045 |
| $\mu$, mm$^{-1}$ | 1.356 | 0.7274 | 0.6953 | 1.616 |
| *T*, K | 90 | 90 | 90 | 90 |
| $\lambda$, Å | 0.71073 | 0.71073 | 0.71073 | 0.71073 |
| R1 | 0.0525 | 0.0735 | 0.0771 | 0.0340 |
| wR2 | 0.1510 | 0.1619 | 0.1378 | 0.0830 |

**Table 2.** Selected Bond Lengths (Å) and Valence Sums[44] of the Vanadium Ions for the Oxides of This Study

| | **1a** | **2** | **3** | **4a** | | **5** | | **6a** | | **7** | | | |
|---|---|---|---|---|---|---|---|---|---|---|---|---|---|
| V−O(oxo) | 1.595(2) | 1.590(3) | 1.579(3) | 1.592(2) | 1.620(3) | 1.596(6) | 1.575(7) | 1.592(3) | | 1.585(2) | 1.588(2) | 1.585(2) | |
| V−O (phosphonate) | 1.948(1) × 2 | 1.971(2) | 2.031(2) × 4 | 1.951(2) | 1.976(2) | 1.954(5) | 1.936(5) | 1.945(3) | | 1.952(2) | 1.958(2) | 1.952(2) | |
| | 2.057(1) × 2 | 1.998(2) | | 1.966(2) | 1.980(2) | 1.972(5) | 1.958(5) | 1.950(3) | | 1.957(2) | 1.959(2) | 1.957(2) | |
| | | 2.058(2) | | 1.996(2) | 1.995(2) | 1.982(6) | 1.977(5) | 1.968(3) | | 1.990(2) | 1.966(2) | 1.987(2) | |
| | | | | | | 1.990(5) | 1.978(5) | 2.022(3) | | 1.991(2) | 1.967(2) | 1.990(2) | |
| V−O (hydroxide) | | | | 1.942(2) | 1.978(2) | | | | | | | | |
| V−O (aqua) | 2.369(2) | 2.025(2) | | - | 2.421(3) | | | | | | | | |
| | | 2.348(3) | | | | | | | | | | | |
| Σs[42] | 3.91 | 3.98 | 3.83 | 4.14 | 4.08 | 4.06 | 4.13 | 4.09 | | 4.12 | 4.17 | 4.13 | |
| P−O | 1.512(1) × 2 | 1.513(2) | 1.514(2) | 1.524(2) | 1.526(2) | 1.495(5) | 1.519(6) | 1.521(3) | 1.515(3) | 1.515(2) | 1.518(2) | 1.518(2) | 1.515(2) |
| | 1.563(2) | 1.536(2) | 1.522(2) | 1.525(2) | 1.530(2) | 1.521(5) | 1.526(5) | 1.533(3) | 1.523(3) | 1.526(2) | 1.524(2) | 1.525(2) | 1.527(2) |
| | | 1.552(2) | 1.583(1) | 1.536(2) | 1.530(2) | 1.522(5) | 1.526(5) | 1.539(3) | 1.570(3) | 1.534(2) | 1.533(2) | 1.534(2) | 1.536(2) |

organic spacers of the diphosphonate ligand, is adopted by the oxides of types **1**−**6** of this study. The series of compounds **1a**−**d** exhibit a 3-D structure based on the identical 2-D $\{V_2O_2(H_2O)(O_3P-)_2\}$ networks linked through the $-(CH_2)_n-$ chains of the ligand, as shown in Figure 1a,b.[22] The V−P−O layer substructure is constructed from face-sharing pairs of vanadium(IV) octahedra and phosphorus tetrahedra. The vanadium octahedra of the binuclear sites are defined by four oxygen donors from four phosphonate phosphorus groups, a terminal oxo group, and an aqua ligand bridging the vanadium(IV) sites.[44] Each phosphorus tetrahedron links three vanadium binuclear units of a layer with two oxygen donors terminally bound to two vanadium sites of adjacent binuclear units and the third bridging vanadium octahedra of a single binuclear unit. The organic chains of the diphosphonate ligands extend outward from either face of a V−P−O layer and serve to link adjacent layers in a characteristic "pillared" layer architecture. The expansion of the tether length from **1a** to **1d** is reflected not only in the interlamellar separation (**1a**, 4.36 Å; **1b**, 5.71 Å; **1c**, 6.92 Å; **1d**, 8.23 Å) but also in the void volume accessible to solvent molecules. Thus, the number of $H_2O$ molecules of crystallization increases from 1 to 3 as *n* increases from 2 to 5 and the solvent accessible volume per unit cell volume increases from ca. 15% to 23.5%.

Curiously, when $n = 6$, a new structure type is observed, as depicted in Figure 1 c,d. Compound **2** exhibits overall 2-D connectivity, manifested as isolated slabs of 13.47-Å thickness stacked along the *a* axial direction. In this instance, the diphosphonate tethers project from a single face of the V−P−O layer and consequently link to a single adjacent oxide layer. The distance between V−P−O planes of adjacent slabs is 3.28 Å.

The network substructure of **2** is also distinct from that of **1a**−**d** and is constructed from isolated $\{VO_6\}$ octahedra and phosphorus tetrahedra. The vanadium(IV) geometry is defined by three oxygen donors from three phosphonate ligands and an aqua ligand in the oxide plane with a terminal oxo group and an aqua ligand in the axial positions. The axial aqua ligands project into the interlamellar void to generate a highly hydrophilic domain, while the basal aqua group extends into an intralamellar cavity produced by a 6-polyhedral connect or $\{V_3P_3O_6\}$ 12-membered ring. The terminal oxo group is directed into the intralamellar domain.

Each $\{PO_3\}$ terminus of the diphosphonate ligands engages in corner-sharing with three vanadium octahedra of a layer. The organic tether $-(CH_2)_6-$ makes an angle of 77.5° with the V−P−O layers, producing an alignment of linked layers which is one polyhedral unit out of registry. Thus, viewed along the *b* crystallographic axis, a vanadium octahedron of one layer sits above a phosphorus tetrahedron of an adjacent layer.

Further expansion of the tether length to $n = 9$ results in the overall 3-D structure of **3**, shown in Figure 1e,f. The relationship of **3** to **2** is quite clear because once again here are slabs defined by two V−P−O networks tethered by the diphosphonate chains. However, in this instance, the V−P−O networks of adjacent slabs are linked through bridging aqua ligands to produce the overall 3-D connectivity and an unusual V−P−O double layer, two polyhedra in thickness.

Viewed along the *c* axis, there are two repeat distances between V−P−O single layers: 13.49 Å through the nonyl tethers and 17.68 Å through the aqua bridges. The network substructure of **3** is distinct from those of **1** and **2** because each vanadium(IV) octahedron coordinates to four oxygen donors from four phosphonate ligands in the *ab* plane with the terminal oxo group and the aqua ligand in the axial positions.

Each $\{PO_3\}$ terminus of the diphosphonate ligands engages in corner-sharing to two vanadium octahedra, leaving one pendant {P−OH} group at each phosphorus site. The protonation of the O2 site is apparent from the P−O bond distance of 1.583(1) Å, compared to an average distance of 1.518(2) Å for the other P−O bonds, and from the observation of the proton in the final Fourier maps.

The introduction of organonitrogen cations results in dramatic structural perturbations. While compounds **4a**−**k** exhibit the prototypical "pillared" layer architecture (Figure 2a,b**)**, other structural details are quite distinct from those of the series **1a**−**d**. The V−P−O networks consist of corner-sharing pairs of vanadium square pyramids and octahedra and phosphorus tetrahedra. The square-pyramidal geometry is defined by three oxygen donors from three diphosphonate ligands and a bridging hydroxy group in the V−P−O plane

(44) Brown, I. D.; Alternatt, D. *Acta Crystallogr., Sect. C* **1985**, *41*, 244.

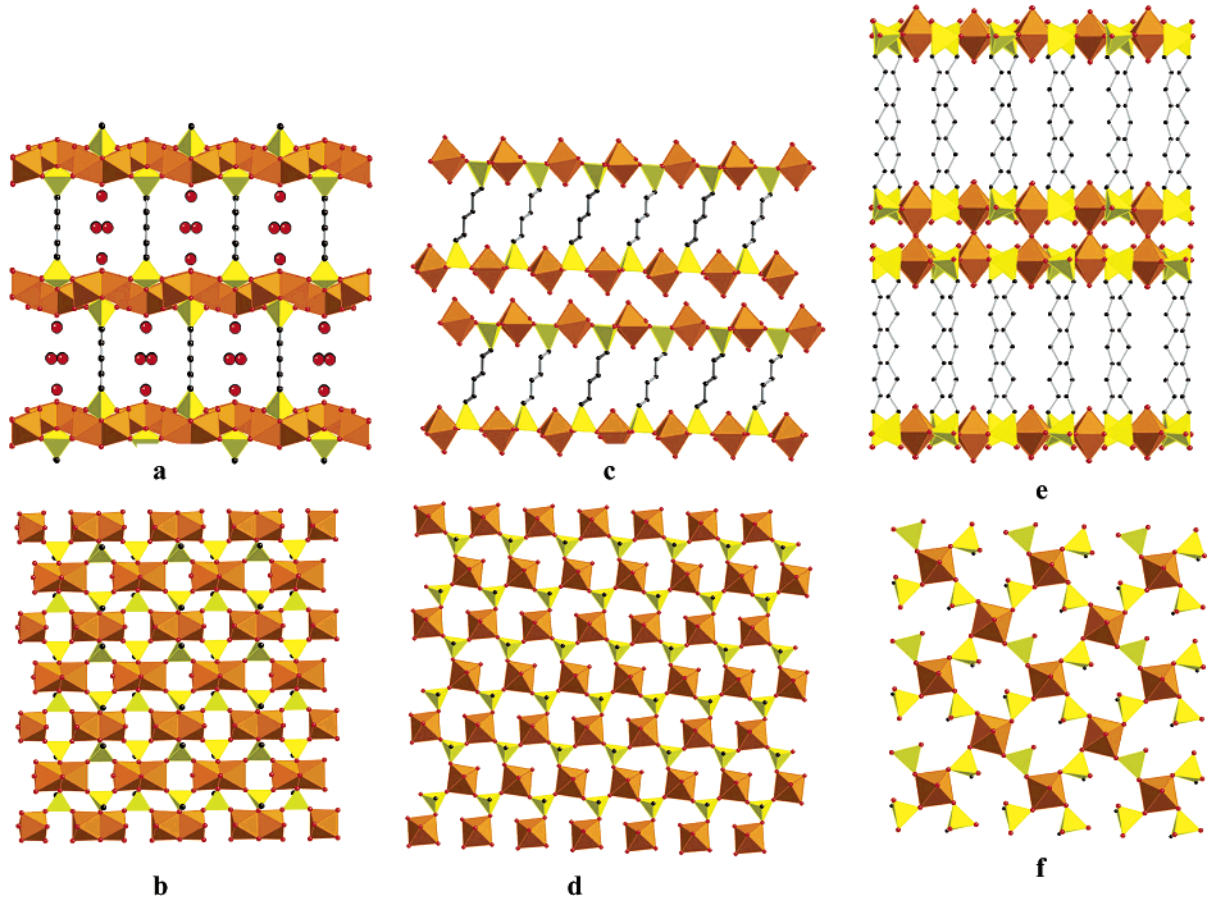


**Figure 1.** Polyhedral representations of the structures of materials of types **1**−**3**, viewed both parallel to the V−P−O plane and normal to the V−P−O plane: (a and b) **1d**; (c and d) **2**; (e and f) **3**.

and an axial oxo group, while the six-coordinate site exhibits the same in-plane coordination but with axial oxo and aqua groups. The oxo groups of the vanadium centers of a binuclear unit adopt the anti orientation with respect to the V−P−O plane and project from either face of the plane into the domains of the organic tethers.

Each phosphorus tetrahedron exhibits corner-sharing to three vanadium polyhedra: the octahedral site of a binuclear unit and both vanadium sites of an adjacent binuclear unit. The polyhedral connectivity generates eight polyhedral connects or $\{V_4P_4O_8\}$ rings, as well as three connects and five connects, $\{V_2PO_3\}$ and $\{V_3P_2O_5\}$ rings, respectively.

The distance between adjacent V−P−O layers of **4d** is 3.15 Å. The interlamellar region is populated by the propylene tethers of the diphosphonate, the cation, and water molecules of crystallization. Thus, the "pillared" layer structure with propylenediphosphonate tethers is persistent and accommodates a variety of charge-compensating organonitrogen cations of considerably different steric requirements: $H_3N(CH_2)_nNH_3$ for $n = 2-7$ (**4a**−**f**), 1,2-diammonium propane (**4g**), and the mononegative anions methyl-, ethyl-, propyl-, and diethylammonium (**4h**−**k**).

Curiously, for tether length $n = 5$, the 2-D **5**, shown in Figure 2c,d, is isolated, for which an analogous structure has been reported for a mixed-valence phase $[NH_4][V_2O_2(OH)(H_2O)\{O_3P(CH_2)_3PO_3\}]\cdot H_2O$.[45] The V−P−O layer structure of **5** is nearly identical with that of the series **4a**−**d** with the exception that the aqua ligand is absent from every other vanadium binuclear unit. Consequently, there are two distinct binuclear vanadium sites: one consisting of a corner-sharing octahedron and square pyramid and the second constructed from a pair of corner-sharing square pyramids. There are two different $\{PO_3\}$ sites associated with the V−P−O layers. One phosphorus tetrahedron bridges two adjacent binuclear vanadium subunits by corner-sharing to the octahedral site of one and to both square-pyramidal sites of the second. The other phosphorus tetrahedron corner-shares to square-pyramidal sites from three neighboring binuclear subunits. The polyhedral connectivity pattern produces eight connect rings $\{V_4P_4O_8\}$, as well as smaller three connects $\{V_2PO_3\}$, four connects $\{V_2P_2O_4\}$, and five connects $\{V_3P_2O_5\}$.

Because the tether groups of the diphosphonate ligands project from a single face of the V−P−O network, a 2-D slab structure with the pentyl tethers sandwiched between two V−P−O layers is observed. The cations are located in the interlamellar domain with one $\{NH_3\}^+$ terminus directed into the larger $\{V_4P_4O_8\}$ ring of the V−P−O network. The stacking of slabs along the *a* axis produces alternating repeats

(45) Riou, D.; Ferey, G. *J. Mater. Chem.* **1998**, *8*, 2733.

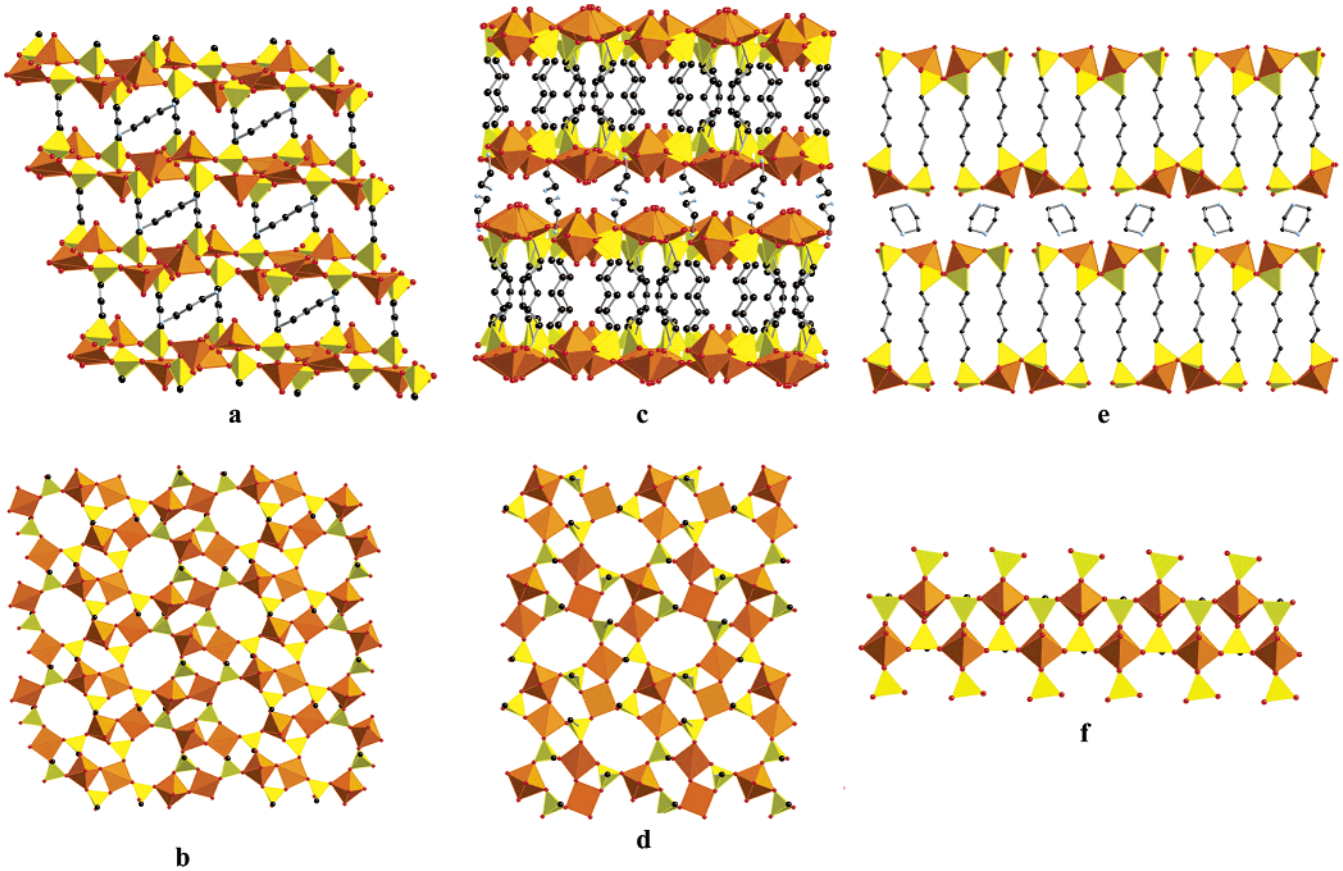


**Figure 2.** Polyhedral representations of the structures of materials of types **4**−**6**, viewed both parallel and normal to the V−P−O planes: (a and b) **4b**; (c and d) **5**; (e and f) **6c**.

of 14.17 Å between the two layers defining the slab surfaces and 2.05 Å between slabs.

The use of a piperazinium cation results in yet another series of 2-D compounds, **6a**−**c**. As shown in Figure 2e,f, the structures are reminiscent of that previously described for **2** but with significant differences in detail. The structure of **6c** consists of slabs constructed of V−P−O chains linked through the diphosphonate tethers. The vanadium geometry is defined by four phosphonate oxygen donors in the basal plane and an apical oxo group, which projects into the interlamellar region rather than into the intralamellar domain as observed for **2** and **3**. The V−P−O substructure of **6a**−**c** is an unusual chain of vanadium(IV) square pyramids and phosphorus tetrahedra. While one phosphorus terminus of a diphosphonate ligand bridges three vanadium sites, the second phosphorus terminus bonds to a single vanadium and exhibits pendant P═O and P−OH groups, with P−O distances of 1.503(3) and 1.575(3) Å, respectively. The result is a distinctly undulating 2-D substructure with $\{VO(O_3P-)(HO_3P-)\}_n^{n-}$ chains running parallel to the *c* axis. The piperazinium cations occupy the interlamellar region and exhibit hydrogen bonding to the pendant P═O groups with N−L−O distances of 2.744(3) Å.

A unique 3-D framework structure is observed for **7**, as shown in Figure 3. The structure consists of a 3-D V−P−O substructure generating channels of dimensions 10.4 Å × 8.0 Å occupied by the cations. The unusual connectivity is dictated, in part, by the ability of the short-chain ethylene-

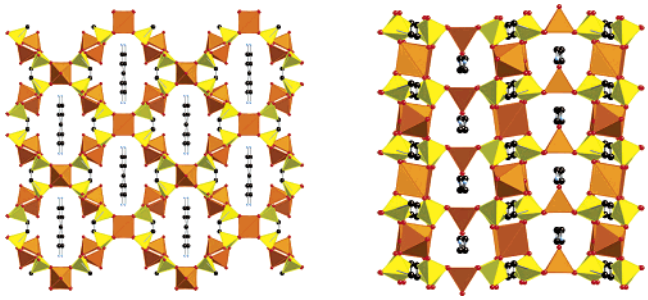

**Figure 3.** Two views of the 3-D structure of **7**.

diphosphonate to adopt a chelating role through oxygen donors at each phosphorus terminus in forming 7-membered [V(O−P−C−C−P−O−)] rings. One vanadium(IV) square pyramid is coordinated in this fashion to two diphosphonate ligands, which use their remaining oxygen donors to bond to four neighboring vanadium(IV) sites in the conventional fashion. Alternatively, the structure may be described as $[VO\{O_3P(CH_2)_2PO_3\}]_n^{2-}$ layers parallel to the *bc* plane linked through $\{VO_5\}$ square pyramids. The terminal oxo groups of the vanadium sites of these virtual layers project into the large cavities occupied by the cations, while the oxo groups of the chelated vanadium sites project between cations into a smaller channel running parallel to the *b* axis. The periphery of the large cavity is defined by a 30-membered $\{V_6P_8O_{12}C_4\}$ ring, while the smaller channel is bound by an 8-polyhedral connect, that is, a $\{V_4P_4O_8\}$ ring.

The compounds of this study are representative examples of the growing family of oxovanadium diphosphonate materials, listed in Table 3.[46−53] Although the "pillared" layer motif is a recurrent theme of the structural chemistry of these metal−oxide hybrids, there are several subgroups that do not conform to this prototype. The first are phases incorporating methylenediphosphonate building blocks. As previously noted,[54] the short spacer length of this ligand favors chelation to a metal with the formation of {M−O−P−C−P−O−} 6-membered rings, which precludes pillaring of adjacent M−P−O layers. Consequently, spatial expansion of the structure occurs through a variety of bridging modes, resulting in a complex structural chemistry represented by 1-, 2-, and 3-D structures. The constituent V−P−O substructures span the range of isolated $\{VO(O_3PCH_2PO_3)_2\}$ subunits to chains, networks, and frameworks. It is noteworthy that ethylenediphosphonate represents the transitional spacer length between extension via pillaring and chelation of metal sites, again resulting a range of structural types.

The second persistent exception to pillaring occurs when $\{Cu_2(bisterpy)\}^{4+}$ is used as the charge-balancing component. Because this secondary metal coordination complex also functions as a dipodal linker between V−P−O subunits, the tendency to form V−P−O layers appears to be disrupted. Consequently, rather than forming the common motif of Chart 1, spatial expansion is achieved by linking smaller V−P−O subunits through both the diphosphonate and the $\{Cu_2(bisterpy)\}^{4+}$ subunits, as shown in Chart 2.

While "pillared" layer structures are most commonly observed for the oxovanadium diphosphonate materials, it is apparent that there are considerable variations in the details of these structures. In terms of the spatial expansion of the structure, two subclasses are observed, 3-D structures and 2-D slabs, depending on whether the organic tethers project from both faces of the V−P−O network substructure or from a single face, respectively. This characteristic feature of the structural chemistry is evident in the contrasting structures of compounds of types **1** and **2** of this study. It is noteworthy that the slablike motifs of V−P−O faces sandwiching organic tethers may fuse through V−O−V interactions to generate 3-D materials with V−P−O double layers tethered by the organic spacers, as demonstrated by structure **3**.

Within the two subclasses of "pillared" layer materials, the detailed polyhedral connectivities within the V−P−O networks span a range of possibilities reflecting the variety of structural determinants that may come into play. The most obvious of these is the vanadium oxidation state, which may be 3+, 4+, and/or 5+. Reduction to the 4+ oxidation state and even the 3+ oxidation state from vanadium(V) starting materials is not uncommon in the presence of nitrogenous ligands and/or HF. Consequently, variability of coordination polyhedra is introduced: distorted octahedral, square pyramidal, trigonal bipyramidal, and tetrahedral for vanadium(V); distorted octahedral and square pyramidal for vanadium(IV); and regular octahedral for vanadium(III). It is curious that reduced sites, vanadium(IV) and vanadium(III), are the rule, with the exception of the materials incorporating the $\{Cu_2(bisterpy)\}^{4+}$ secondary metal coordination cation (SMCC), where vanadium(V) sites are almost exclusively entrained. Because the redox potential of bisterpy is not significantly different from those of terpy, bpy, and other organonitrogen components and because HF is also introduced in the syntheses of the materials containing $\{Cu_2(bisterpy)\}^{4+}$, the rationale for this observation remains elusive.

The details of the V−P−O network structures reflect not only the vanadium polyhedral type or types present but also the extent of condensation of vanadium polyhedra through V−O−V bonding. Thus, the broad family of materials features isolated vanadium sites, binuclear and trinuclear clusters, and vanadate chains. The polyhedra may also fuse through corner-, edge-, or face-sharing interactions.

Another common characteristic of the vanadium coordination is the incorporation of $H_2O$ or hydroxide ligands. While this feature adds significantly to the potential structural diversity, it is unpredictable and uncontrollable under our reaction conditions.

Similarly, the polyhedral connectivities adopted by the $\{PO_3\}$ termini of the diphosphonate ligand are variable. Thus, the $\{PO_3\}$ unit may share three vertexes with vanadium sites, two with a pendant {P−OH} group, or one with pendant {P═O} and {P−OH} units or, on rare occasions, it may be present as a pendant $\{-PO_3H_2\}$ group. This represents a significant structural determinant because P−O or P−OH bond distances also span a range of 1.45−1.62 Å.[55] Furthermore, the V−O−P angle is "soft", spanning a range of 30° and allowing considerable flexibility in the polymerization of polyhedra in generating the overall architecture.

The charge of the V−P−O network also dictates the structure. As shown in Figures 1 and 2, the structures of the neutral V−P−O networks are quite distinct from those of the anionic series. In general, the neutral V−P−O networks are more dense than those of the anionic series, which exhibit vacancies in the form of large polyhedral connect rings or even disruption of the layer into chains (type **7**). This feature of the anionic V−P−O networks appears to be related to the need to accommodate the positively charged terminus of the organoammonium cations, either within the layer or just above a face of the V−P−O network. The observed structures may consequently reflect the requirements of charge-density matching.[56,57]

(46) Huan, G.; Johnson, J. W.; Jacobson, A. J. *J. Solid State Chem.* **1990**, *89*, 220.
(47) Riou, D.; Serre, C.; Ferey, G. *J. Solid State Chem.* **1998**, *141*, 89.
(48) Ninclaus, C.; Serre, C.; Riou, D.; Ferey, G. *C. R. Acad. Sci., Ser. IIc: Chim.* **1998**, *1*, 551.
(49) Riou, D.; Roubeau, O.; Ferey, G. *Microporous Mesoporous Mater.* **1998**, *23*, 23.
(50) Finn, R. C.; Zubieta, J. *Dalton Trans.* **2000**, 1821.
(51) Finn, R. C.; Lam, R.; Greedan, J. E.; Zubieta, J. *Inorg. Chem.* **2001**, *40*, 3745.
(52) Finn, R. C.; Zubieta, J. *Inorg. Chem. Commun.* **2000**, *3*, 520.
(53) Ouellette, W.; Koo, B.-K.; Burkholder, E.; Golub, V.; O'Connor, C. J.; Zubieta, J. *Dalton Trans.* **2004**, 1527.
(54) Burkholder, E.; Golub, V.; O'Connor, C. J.; Zubieta, J. *Inorg. Chem.* **2004**, *43*, 7014.
(55) Huminichi, D. M. C.; Hawthorne, F. C. *Rev. Mineral. Geochem.* **2002**, *48*, 123.

**Table 3.** Selected Structural Characteristics and Component Building Blocks of Oxovanadium Diphosphonate Compounds

| compound | overall dimens | description | vanadium building blocks | other characteristics | ref |
|---|---|---|---|---|---|
| | | I. Neutral V−P−O Substructure | | | |
| $[V_2O_2(H_2O)_2\{O_3PCH_2PO_3\}_2]$ | 2-D | V−P−O network | isolated vanadium(IV) octahedra | coordinated $H_2O$ | 46 |
| $[V(HO_3PCH_2CH_2PO_3)(H_2O)]$ | 3-D | V−P−O framework | isolated vanadium(III) octahedra | coordinated $H_2O$ | 20 |
| $[V_2O_2(H_2O)\{O_3P(CH_2)_nPO_3\}]\cdot xH_2O$ (**1a**−**d**) | 3-D | pillared V−P−O network | binuclear units of edge-sharing vanadium(IV) octahedra | coordinated $H_2O$ | this work, 22 |
| $[V_2O_2(H_2O)_4\{O_3P(CH_2)_6PO_3\}]$ (**2**) | 2-D | pillared V−P−O networks sandwiching the organic tethers | isolated vanadium(IV) octahedra | coordinated $H_2O$ | this work |
| $[V_2O_2(H_2O)\{HO_3P(CH_2)_9PO_3\}_2]$ (**3**) | 3-D | pillared V−P−O double layers | binuclear units of corner-sharing vanadium(IV) octahedra | coordinated $H_2O$ | this work |
| $[V_2O_2(OH)\{O_3PCH_2CH_2PO_3\}]\cdot H_2O$ | 3-D | pillared V−P−O networks | binuclear units of face-sharing vanadium(IV)/vanadium(V) octahedra | coordinated $OH^-$ | 47 |
| | | II. Anionic V−P−O Substructures | | | |
| $(NH_4)_2[VO\{O_3PCH_2PO_3\}]$ | 1-D | V−P−O chain | chains of corner-sharing vanadium(IV) octahedra | V···O═V···O chains | 48 |
| $Cs[VO\{O_3PCH_2PO_3\}]$ | 1-D | V−P−O chain | chains of corner-sharing vanadium(IV) octahedra | V···O═V···O chains | 20 |
| $(H_2pip)[VO\{O_3PCH_2PO_3\}]$ | 1-D | $\{VO(O_3P\text{-})_4\}$ subunits | isolated vanadium(IV) square pyramids | | 17 |
| $Cs[V_3O_2(H_2O)_2\{O_3PCH_2PO_3\}_2]$ | 2-D | V−P−O double layer | trinuclear units of corner-sharing vanadium(IV)/vanadium(III) octahedra | O═V−O···V···O−V═O units; coordinated $H_2O$ | 20 |
| $(NH_4)_4[V_6O_6(H_2O)_4\{O_3PCH_2PO_3\}_4]$ | 3-D | pillared V−P−O networks | isolated vanadium(IV) octahedra and vanadium(V) square pyramids | coordinated $H_2O$ | 49 |
| $(H_2en)[VO\{O_3PCH_2CH_2PO_3\}]$ | 2-D | V−P−O chains | isolated vanadium(IV) square pyramids | | 17 |
| $Cs[V_2O_2(OH)\{O_3PCH_2CH_2PO_3\}]$ | 2-D | pillared V−P−O networks sandwiching the organic tethers | binuclear units of corner-sharing vanadium(IV) square pyramids | coordinated $OH^-$ | 21 |
| $(H_3O)_2[V_3O(OH)_2\{O_3PCH_2CH_2PO_3\}]\cdot H_2O$ | 3-D | pillared V−P−O networks | chains of corner-sharing vanadium(III) octahedra and isolated vanadium(IV) square pyramids | coordinated $OH^-$ | 17 |
| $(H_3O)[V_3\{O_3PCH_2CH_2PO_3\}\{HO_3PCH_2CH_2PO_3H\}_3]\cdot xH_2O$ | 3-D | pillared V−P−O networks | isolated vanadium(III) octahedra | | 19 |
| $(NH_4)[V_2O_3(H_2O)\{O_3P(CH_2)_3PO_3\}]\cdot 2H_2O$ | 3-D | pillared V−P−O networks | binuclear units of corner-sharing vanadium(IV) octahedra and vanadium(V) square pyramids | coordinated $H_2O$ | 45 |
| $(NH_4)[V_2O_2(OH)(H_2O)\{O_3P(CH_2)_3PO_3\}]\cdot 2H_2O$ | 3-D | pillared V−P−O networks | binuclear units of corner-sharing vanadium(IV) octahedra and square pyramids | coordinated $H_2O$ and $OH^-$ | 45 |
| $(H_2pip)[V_2O_2\{O_3P(CH_2)_3PO_3H\}_2]$ | 2-D | stain-stepped network | isolated vanadium(IV) octahedra | | 18 |
| $[VO(H_2O)\{O_3PC_2H_2NH(C_2H_4)_2NHCH_2PO_3\}]$ | 3-D | pillared V−P−O networks | isolated vanadium(IV) octahedra | coordinated $H_2O$ | 18 |
| $(cat.)[V_4O_6(OH)_2\{O_3P(CH_2)_3PO_3\}_2]\cdot xH_2O$ (**4a**−**g**) | 3-D | pillared V−P−O networks | binuclear units of corner-sharing vanadium(IV) octahedra and square pyramids | coordinated $OH^-$ | this work |
| $(H_2en)[V_4O_4(OH)_2(H_2O)_2\{O_3P(CH_3)_3PO_3\}_2]\cdot 4H_2O$ | 3-D | pillared V−P−O networks | binuclear units of corner-sharing vanadium(IV) octahedra and square pyramids | coordinated $H_2O$ and $HO^-$ | 17 |
| $[H_3N(CH_2)_2NH_3][V_4O_4(OH)_2(H_2O)\{O_3P(CH_2)_5PO_3\}_2]\cdot H_2O$ (**5**) | 2-D | pillared V−P−O networks sandwiching the organic tethers | binuclear units of corner-sharing vanadium(IV) square pyramids; binuclear units of corner-sharing vanadium(IV) octahedra and square pyramids | coordinated $H_2O$ and $OH^-$ | this work |
| $[H_2N(CH_2CH_2)_2NH_2][V_2O_2\{O_3P(CH_2)_nPO_3H\}_2]$ (**6a**−**c**) | 2-D | Folded layers of tethered $[VO\{O_3P(CH_2)_nPO_3H\}]_n$ chains | isolated vanadium(IV) square pyramids | | this work |
| $[H_3N(CH_2)_5NH_3][V_3O_3\{O_3P(CH_2)_2PO_3\}_2]$ (**7**) | 3-D | V−P−O framework | isolated vanadium(IV) square pyramids | | this work |
| | | III. Anionic V−P−O− Substructures with SMCC as a Charge-Balancing Component | | | |
| $[\{Cu(2,2'\text{-bpy})(H_2O)\}VO\{O_3PCH_2PO_3\}]$ | 2-D | $[VO\{O_3PCH_2PO_3\}]_n^{2n-}$ network | isolated vanadium(IV) square pyramids | no V−O−Cu bonding | 50 |
| $[\{Cu(2,2'\text{-bpy})\{VO\{O_3P(CH_2)_nPO_3\}\}]$ | 3-D | pillared V−P−O networks | isolated vanadium(IV) square pyramids | V−O−Cu bonding | 50 |
| $[\{Cu(phen)\}VO(H_2O)\{O_3PCH_2PO_3\}]$ | 2-D | $[VO(H_2O)\{O_3PCH_2PO_3\}]_n^{2n-}$ chains linked through copper(II) sites | isolated vanadium(IV) square pyramids | no V−O−Cu bonding, coordinated $H_2O$ | 51 |

**Table 3.** (Continued)

| compound | overall dimens | description | vanadium building blocks | other characteristics | ref |
|---|---|---|---|---|---|
| III. Anionic V−P−O− Substructures with SMCC as a Charge-Balancing Component (Continued) | | | | | |
| $[\{Cu(bpy\text{-}dicarb)\}_2V_3O_3(OH)_2(H_2O)\{O_3PCH_2PO_3\}_2]$ | 2-D | $[V_3O_3(OH)_2(H_2O)\{O_3PCH_2PO_3\}_2]_n^{4n-}$ network | trinuclear units of a central vanadium(IV) octahedron and two peripheral vanadium(IV) square pyramids | coordinated $H_2O$ and $OH^-$ V−O−Cu bonding | 52 |
| $[\{Cu(phen)\}_2V_2O_5\{O_3PCH_2CH_2PO_3\}]$ | 2-D | $[V_2O_5\{O_3PCH_2CH_2PO_3\}]_n^{4n-}$ chains linked through copper(III) sites | binuclear units of corner-sharing vanadium(V) tetrahedra | V−O−Cu bonding | 51 |
| $[\{Cu(phen)\}_2V_4O_5(H_2O)\{O_3P(CH_2)_3PO_3\}]$ | 2-D | $[V_3O_5(H_2O)\{O_3P(CH_2)_3PO_3\}]_n^{4n-}$ networks decorated with copper(II) units | trinuclear units of a central vanadium(IV) octahedron and two peripheral vanadium(V) square pyramids | coordinated $H_2O$; V−O−Cu bonding | 51 |
| $[\{Cu(phen)\}_2V_3O_5(H_2O)\{O_3PCH_2PO_3\}]$ | 3-D | $[V_3O_5(H_2O)\{O_3PCH_2PO_3\}]_n^{4n-}$ framework with embedded $\{Cu^{II}(phen)\}^{2+}$ units | isolated vanadium(IV) octahedra and vanadium(V) tetrahedra | coordinated $H_2O$; V−O−Cu bonding | 51 |
| $[\{Cu_2(bisterpy)V_2O_4\{O_3PCH_2PO_3H\}_2]$ | 1-D | $[V_2O_4\{O_3PCH_2PO_3H\}_2]^{4-}$ cluster linked through $\{Cu_2(bisterpy)\}^{4+}$ units | isolated vanadium(V) trigonal bipyramids | no V−O−Cu bonding | 53 |
| $[\{Cu_2(bisterpy)\}V_2O_4\{O_3PCH_2CH_2PO_3H\}_2]$ | 2-D | $[V_2O_4\{O_3PCH_2CH_2PO_3H\}_2]_n^{4n-}$ chains | isolated vanadium(V) square pyramids | no V−O−Cu bonding | 53 |
| $[\{Cu_2(bisterpy)\}V_4O_8\{O_3P(CH_2)_3PO_3\}_2]\cdot 4H_2O$ | 2-D | $[V_2O_4\{O_3P(CH_2)_3PO_3\}_2]_n^{4n-}$ chains | isolated vanadium(V) square pyramids | V−O−Cu bonding | 53 |
| $[\{Cu_2(bisterpy)(H_2O)\}VO_2\{O_3P(CH_2)_3PO_3\}\{HO_3P(CH_2)_3PO_3H_2\}]$ | 1-D | $[V_2O_4\{O_3P(CH_2)_3PO_3\}]^{2-}$ clusters | isolated vanadium(V) tetrahedra | no V−O−Cu bonding | 53 |
| $[\{Cu_2(bisterpy)\}V_2O_4(OH)_2\{O_3P(CH_2)_4PO_3\}]\cdot 4H_2O$ | 2-D | $[V_2O_4\{O_3P(CH_2)_4PO_3\}]^{4-}$ clusters | isolated vanadium(V) tetrahedra | no V−O−Cu bonding | 53 |
| $[\{Cu_2(bisterpy)\}V_4O_4\{O_3P(CH_2)_5PO_3H\}_4]\cdot 7H_2O$ | 3-D | $[VO\{O_3P(CH_2)_5PO_3H\}]_n^{n-}$ framework | isolated vanadium(IV) square pyramids | V−O−Cu bonding | 53 |
| $[\{Cu_2(bisterpy)\}V_2O_4\{O_3P(CH_2)_6PO_3H\}_2]\cdot 2H_2O$ | 1-D | $[V_2O_4\{O_3P(CH_2)_6PO_3H\}_2]^{4-}$ cluster | isolated vanadium(V) trigonal bipyramids | V−O−Cu bonding | 53 |

**Chart 2**

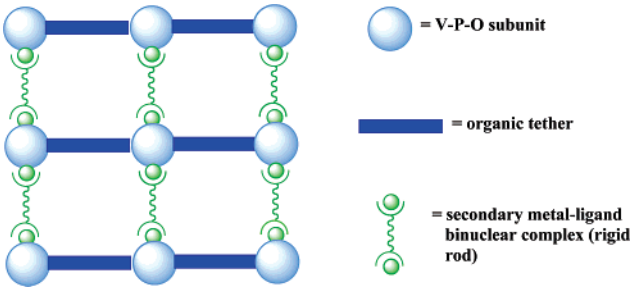


The identity of the cation also serves as a structural determinant, as is clearly demonstrated in the grossly different structures observed for phases with simple inorganic cations such as $NH_4^+$, $Cs^+$, and $H_3O^+$, those with SMCC cations, and those incorporating organoammonium cations. Even when our attention is restricted to the latter series of this study, the contrast between structures incorporating single-chain $\{H_3N(CH_2)_nNH_3\}^{2+}$ cations (type **4**) and piperazinium cations (type **6**) is stark. However, it is also noteworthy that, for the series with propylenediphosphonate (type **4**), the architecture is insensitive to the organodiammonium cation chain length, at least up to $n = 7$. This reflects the large intralamellar void space, which can readily accommodate the organic cation in one of the two distinct domains. It is also noteworthy that, as the chain length of the organodiammonium cation increases and this unit begins to spill over into the adjacent hydrophilic cavity, the amount of water of crystallization entrained within the latter cavity decreases. In the series $[H_3N(CH_2)_nNH_3][V_4O_4(OH)_2\{O_3P(CH_2)_3PO_3\}_2]\cdot xH_2O$, it is noted that, for $n = 2$, $x = 6$, while at the other extreme, for $n = 7$, $x = 0$.

Finally, the structures reflect the spacer lengths of the diphosphonate ligands. This is most readily apparent in comparing structures **1**−**3**. Thus, structure type **1**, $[V_2O_2(H_2O)\{O_3P(CH_2)_nPO_3\}]\cdot xH_2O$ (**1a**−**d**), persists for $n = 2$−5. At $n = 6$, structure type **2** is adopted and retained for $n = 7$ and 8, while at $n = 9$, structure type **3**, $[V_2O_2(H_2O)\{HO_3P(CH_2)_9PO_3H\}_2]$, is observed. Similarly, for the V−P−O anionic frameworks, structure type **4**, $[H_3N(CH_2)_5NH_3][V_4O_4(OH)_2\{O_3P(CH_2)_nPO_3\}_2]$, is observed for $n = 3$, while structure **7**, $[H_3N(CH_2)_5NH_3][V_3O_3\{O_3P(CH_2)_nPO_3\}_2]$, results for $n = 2$.

**Magnetism**. The structural diversity of the compounds of this study is reflected in the physical properties, such as porosity and long-range magnetic interactions. Metal−oxide hybrids afford the opportunity to study magnetically condensed (exchange-coupled) systems.[58] Low-dimensional arrangements of the magnetic ions may be attained through the use of nonmagnetic dividers such as the organic subunits.[59]

The dependence of magnetic susceptibility $\chi$ and effective magnetic moment $\mu_{eff}$ on the temperature for **1d** is shown in Figure 4. The magnetic susceptibility is best described by

(56) Monnier, A.; Schuth, F.; Huo, Q.; Kumar, D.; Margolese, D.; Maxwell, R. S.; Stucky, G. D.; Krishnamurty, M.; Petroff, P.; Firouz, A.; Janicke, M.; Chmelka, B. F. *Science* **1993**, *216*, 1299.
(57) Maggard, P. A.; Boyle, P. D. *Inorg. Chem.* **2003**, *42*, 4250.
(58) Drillon, M.; Panissod, P. *J. Magn. Mater.* **1998**, *188*, 93.
(59) Rarig, R. S.; Lam, R.; Zawalij, P. Y.; Ngala, J. K.; LaDuca, R. L.; Greedan, J. E.; Zubieta, J. *Inorg. Chem.* **2002**, *41*, 2124.

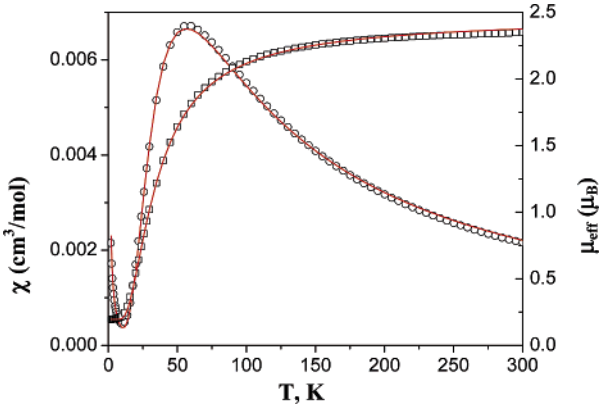


**Figure 4.** Dependence of the magnetic susceptibility $\chi$ (○) and of the effective moment $\mu_{eff}$ (□) of **1d** on the temperature. The lines drawn through the data are the fits to the Heisenberg dimer model.

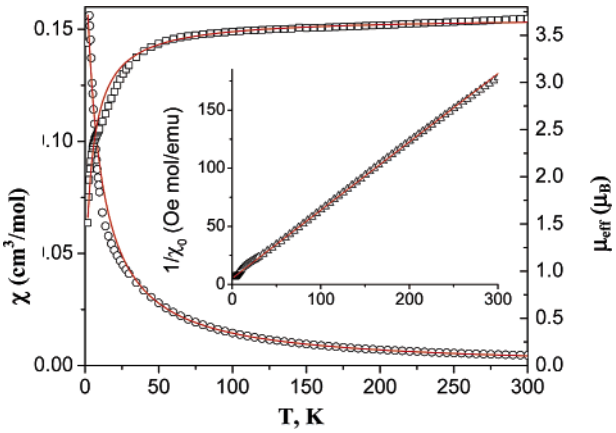


**Figure 5.** Dependence of the magnetic susceptibility $\chi$ (○) and of the effective moment $\mu_{eff}$ (□) of **4d** on the temperature. The lines drawn through the data are the fits to the Curie−Weiss law.

the Heisenberg dimer model with $S = 1$ (eq 1). The best fit

$$\chi = (1-p)\frac{N_A g^2 \mu_B{}^2}{k_B T}\frac{2\exp(2J/k_B T)}{1+3\exp(2J/k_B T)} + p\frac{N_A g^2 \mu_B{}^2}{2k_B T} + \chi_{TI} \quad (1)$$

to the data gave $g = 2.02$, $J/k_B = -45.6$ K, $\chi_{TI} = -0.000\,14$ emu Oe$^{-1}$ mol$^{-1}$, and $p = 0.0001$. The effective magnetic moment (eq 2) at 300 K is $\mu_{eff}(300\text{ K}) = 2.38\ \mu_B$, which is consistent with two $d^1$ vanadium(IV) ions, each with $S = {}^1/_2$. The analogous compounds **1a** and **1c** exhibit similar

$$\mu_{eff} = \sqrt{8\chi_0 T} \quad (2)$$

magnetic behavior with $g = 1.97$, $J/k_B = -47.3$ K, $\chi_{TI} = 0.0001$ emu Oe$^{-1}$ mol$^{-1}$, $p = 0.010$, and $\mu_{eff}(300\text{ K}) = 2.29\ \mu_B$ for **1a** and $g = 2.00$, $J/k_B = -49.1$ K, $\chi_{TI} = -0.000\,02$ emu Oe$^{-1}$ mol$^{-1}$, $p = 0.001$, and $\mu_{eff}(300\text{ K}) = 2.30\ \mu_B$ for **1c**.

In contrast, the anionic V−P−O network materials of types **4**, **5**, and **7** exhibit Curie−Weiss behavior (eq 3) at higher temperatures, as illustrated in Figure 5 for **4d**. For compound

$$\chi = \chi_0 + \chi_{TI} = \frac{C}{T-\theta} + \chi_{TI} \quad (3)$$

**4d**, the best fit gave $C = 1.70$ emu K Oe$^{-1}$ mol$^{-1}$, $\Theta = -8.9$ K, and $\chi_{TI} = -0.0012$ emu Oe$^{-1}$ mol$^{-1}$. The effective magnetic moment at 300 K was $\mu_{eff}(300\text{ K}) = 3.67\ \mu_B$, corresponding to four vanadium(IV) ions, each with $S = {}^1/_2$, for $g = 2.12$. For compound **4a**, the best fit provided $C = 1.72$ emu K Oe$^{-1}$ mol$^{-1}$, $\Theta = -8.8$ K, and $\chi_{TI} = -0.000\,03$ emu Oe$^{-1}$ mol$^{-1}$, with $\mu_{eff}(300\text{ K}) = 3.72\ \mu_B$, while for **4b**, values of $C = 1.77$ emu K Oe$^{-1}$ mol$^{-1}$, $\Theta = -9.1$ K, and $\chi_{TI} = -0.000\,05$ emu Oe$^{-1}$ mol$^{-1}$, with $\mu_{eff}(300\text{ K}) = 3.74\ \mu_B$ for $g = 2.16$, are derived.

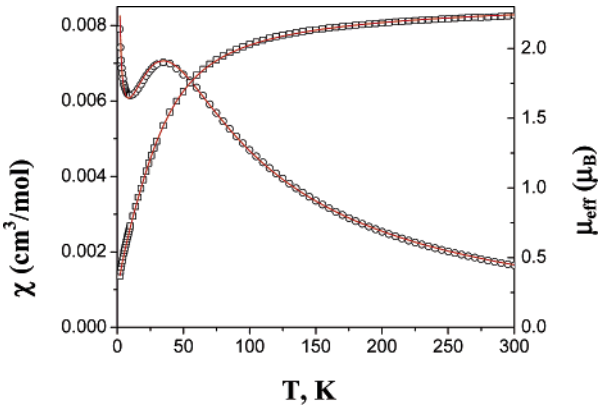


**Figure 6.** Dependence of the magnetic susceptibility $\chi$ (○) and of the effective magnetic moment $\mu_{eff}$ (□) of **6c** on the temperature. The lines drawn through the data are the fits to the Heisenberg antiferromagnetic linear chain model.

For compound **5**, the best fit gave $C = 1.57$ emu K Oe$^{-1}$ mol$^{-1}$, $\Theta = -3.8$ K, and $\chi_{TI} = -0.001\,03$ emu Oe$^{-1}$ mol$^{-1}$. The effective magnetic moment $\mu_{eff}(300\text{ K})$ is 3.57 $\mu_B$ for $g = 2.06$, corresponding to four vanadium(IV) sites, each with $S = {}^1/_2$. In the case of **7**, the susceptibility behavior was consistent with $C = 1.11$ emu K Oe$^{-1}$ mol$^{-1}$, $\Theta = -4.7$ K, and $\chi_{TI} = -0.000\,47$ emu Oe$^{-1}$ mol$^{-1}$. The effective magnetic moment $\mu_{eff}(300\text{ K})$ of 2.96 $\mu_B$ for $g = 1.98$ corresponds to three vanadium(IV) sites.

As shown in Figure 6, the magnetic susceptibility of **6c** exhibits a maximum at 30 K, indicative of the presence of antiferromagnetic interactions. The best description of the experimental results has been obtained with the Heisenberg linear antiferromagnetic chain model ($S = {}^1/_2$; eq 4), taking into account the presence of monomeric paramagnetic impurities of concentrated $p$. The best fit gave $g = 1.92$,

$$c = \frac{2N_A g^2 \mu_B{}^2}{k_B T} \times \left[(1-p)\frac{0.25 + 0.14995y + 0.30094y^2}{1 + 1.9862y + 0.68854y^2 + 6.062y^3} + p/4\right] = \chi_{TI} \quad (4)$$

$J/k_B = -25.7$ K, $\chi_{TI} = -0.0003$ emu Oe$^{-1}$ mol$^{-1}$, and $p = 0.0015$. The effective magnetic moment $\mu_{eff}(300\text{ K})$ is 2.19 $\mu_B$. For the analogous **6a**, the values are $g = 1.96$, $J/k_B = -28.0$ K, $\chi_{TI} = -0.000\,44$ emu Oe$^{-1}$ mol$^{-1}$, $p = 0.01$, and $\mu_{eff}(300\text{ K}) = 2.23\ \mu_B$.

**Thermal Analyses**. The TGA profiles of the oxides of type **1** are characterized by the loss of water of crystallization and coordinated water in the 50−240 °C range, with loss of the tether hydrocarbons above 450 °C with concomitant

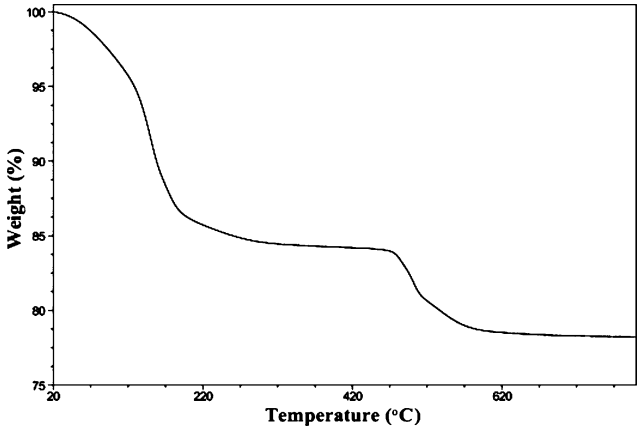


**Figure 7.** TGA curve for **1d**.

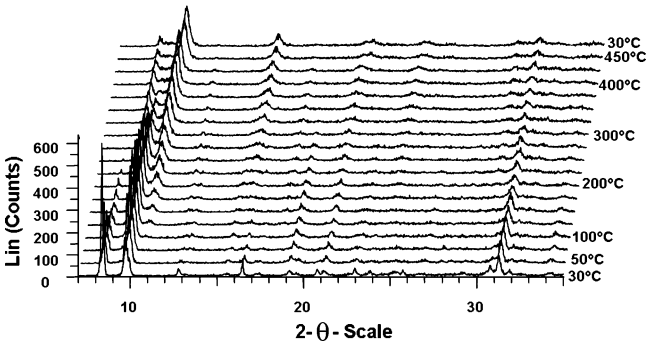


**Figure 8.** Thermodiffraction pattern for **1d** in the 30−425 °C temperature range. Compounds **1a** and **1b** provide similar diffraction patterns.

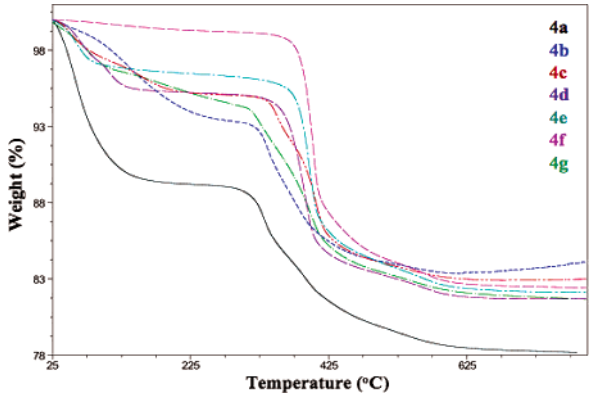


**Figure 9.** Overlay of the TGA curves for **4a**−**g**.

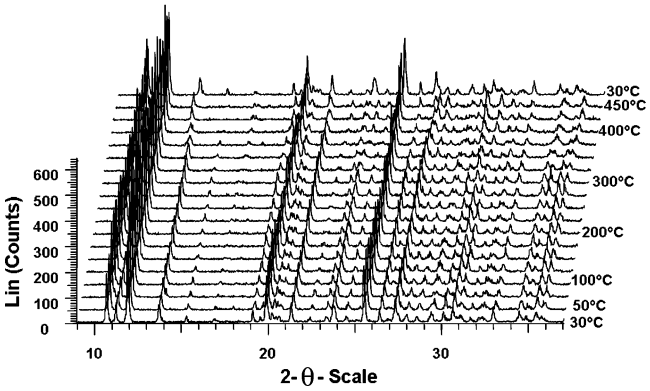


**Figure 10.** Thermodiffraction pattern for **4a** in the 30−425 °C temperature range.

decomposition to an amorphous phase. As shown in Figure 7, for **1d**, there is an initial weight loss from just above room temperature to 190 °C of 16%, corresponding to the loss of four water molecules (16.5%, theoretical weight loss). A second weight loss of ca. 8% corresponds to the loss of hydrocarbon and oxidation of the phosphorus sites (theory: 8.7%). The thermodiffraction pattern for compound **1d** in the temperature range 25−450 °C is shown in Figure 8. The profile indicates that a dehydrated phase isostructural with the parent compound persists to ca. 150 °C, whereupon a second crystalline material is obtained. The structure of the dehydrated phase (**1d′**) does not collapse until temperatures above 450 °C. The thermodiffraction profile of **1d** is consistent with retention of the structure of the parent oxide upon loss of water of crystallization, followed by structural rearrangement concomitant to the loss of the coordinated water molecule.

The compounds of type **4** exhibit more complex TGA profiles, characterized by partial decomposition of the organic cation, as well as dehydration. The representative TGA of **4a**·$6H_2O$ exhibits a weight loss of ca. 12% between room temperature and 100 °C, consistent with the loss of six water molecules of crystallization (theory: 12.5%). This initial weight loss is followed by the loss of the organodiammonium cation in two steps between 250 and 500 °C. The compounds of type **4**, which contain water of crystallization, exhibit TGA profiles similar to that of **4a**, while **4f**, which is devoid of water of crystallization, does not exhibit the initial weight loss (Figure 9). The thermodiffraction pattern for **4a** in the temperature range 25−425 °C shows that the initial profile remains unchanged to at least 400 °C, whereupon only minor changes are observed (Figure 10). Consequently, the initial cation degradation step does not affect the product crystallinity. This observation was confirmed by ramping of a sample of **4a** to 310 °C at 5° $min^{-1}$, whereupon the temperature was maintained at 310 °C for 3 h. No further weight loss was observed after 1 h (Figure 11a). The powder diffraction pattern of this material **4a′** was nearly identical with that of the parent compound **4a**·$6H_2O$, suggesting that the framework of the parent is maintained. The TGA plot of **4a′**, shown in Figure 11b, exhibits a single weight loss from 350 to 600 °C of 16.5%, corresponding to the loss of the remaining cation fragment and the organic residues of the diphosphonate ligand.

The oxide **5**·$0.75H_2O$ exhibits an unexceptional TGA profile. The water of crystallization is lost between room temperature and 80 °C (obsd, 2%; calcd, 1.6%). This is followed by a weight loss of 16% in the 325−590 °C range, corresponding to the loss of the organoammonium cation and of the organic tether and oxidation of the phosphorus sites.

The compounds of type **6**, $[H_2N(CH_2CH_2)_2NH_2][V_2O_2\{O_3P(CH_2)_nPO_3H\}_2]$, are stable to ca. 390 °C, whereupon the organoammonium cation and the organic residues of the diphosphonate ligand are lost. In the case of **6c**, the organic components are lost in two steps. The first weight decrease of ca. 12% is attributed to the loss of the $\{H_2N(CH_2CH_2)_2NH_2\}^{2+}$ cation (calcd: 12.4%), while the second step of ca.

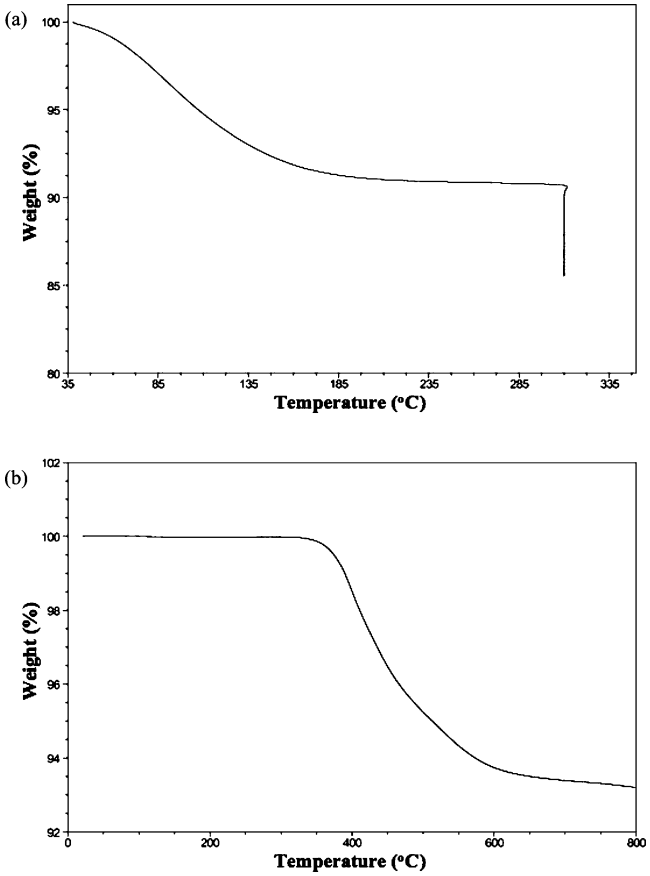


**Figure 11.** (a) TGA of **4a** from room temperature to 310 °C showing that there is no further weight loss from **4a′** when the temperature is held at 310 °C for 3 h. (b) TGA of **4a′** showing the loss of the remaining organic components.

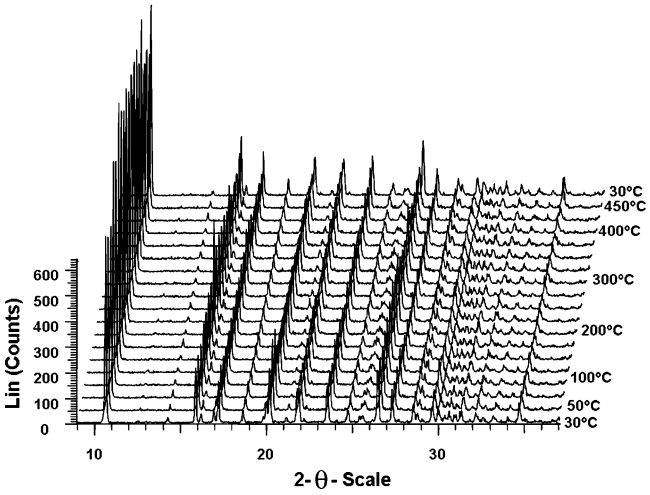


**Figure 12.** Thermodiffraction profile for **6c** in the 30−450 °C range.

10% corresponds to the loss of the organic component of the diphosphonate ligand and oxidation of the phosphorus residues (calcd: 11.3%). The thermodiffraction profile for **6c**, shown in Figure 12, illustrates that the structure of the product of the first thermal process **6c′** is essentially identical with that of the original phase, confirming that the layer structure is retained upon loss of the organoamine component. The thermodiffraction pattern of **6c′** after heating at 450 °C for 1 h and subsequent cooling to room temperature exhibits only minor changes in peak intensities. These observations are confirmed by the IR spectroscopy of **6c** and **6c′**. Compound **6c** exhibits a sharp band at 3050 $cm^{-1}$ attributed to $\nu$(N−H) and a strong absorption associated with N−H scissoring at ca. 1640 $cm^{-1}$. Both peaks are absent from the spectrum of **6c′**, indicating that this thermal process is associated with the loss of the organoamine residues (see the Supporting Information). Elemental analyses of **6c′** confirm the absence of nitrogen in the product and are consistent with a product formulation $[V_2O(OH)\{O_3P(CH_2)_6PO_3H\}_2]$; the crystals of **6c′** are black, suggesting a mixed-valence vanadium(IV)/vanadium(V) material.

Compound **7** is similarly stable to 450 °C, whereupon decomposition to an amorphous phase occurs between 450 and 500 °C.

**Conclusions.** Hydrothermal methods have been exploited in the preparation of two classes of metal−oxide frameworks, the first exhibiting neutral V−P−O networks (types **1**−**3**) and the second based on anionic V−P−O networks or frameworks with entrained organoammonium cations (types **4**−**7**). The structures of these oxovanadium organodiphosphonate phases reveal the persistence of the pillared layer structural motif, which is a recurrent theme of metal organodiphosphonates in general. However, despite the commonality of the gross architecture of these materials, the details of the polyhedral connectivities within the V−P−O networks are quite distinct for types **1**−**7**. The structural determinants include the vanadium oxidation state, the polyhedral variability of the vanadium sites, the oligomerization of vanadium polyhedra through V−O−V interactions, the promiscuous condensation of vanadium and phosphorus polyhedra manifested in the soft V−P−O angles and variable P−O(H) distances, coordination of aqua and hydroxy groups, and the influence of the organic components. It has been noted that incorporation of even small amounts of organic components can profoundly influence the microstructure of inorganic oxides.[60] The structural consequences of the introduction of organic components for compounds **1**−**7** reflect both the tether length of the diphosphonate ligand and the presence and identity of the organoammonium cation.

The influence of the tether length is apparent in the structures of compounds of types **1**−**3**. While type **1** exhibits the conventional 3-D pillared layer architecture, lengthening of the diphosphonate chain $\{O_3P(CH_2)_nPO_3\}^{4-}$ to $n = 6-8$ results in a 2-D pillared slab prototype (type **2**). Further lengthening of the chain to $n = 9$ provides a 3-D structure (type **3**) based on the condensation of V−P−O faces of the slablike structure observed for type **2** oxides.

The structural systematics of the anionic V−P−O networks were influenced by both the identity of the counterion and the spacer length. For chain length $n = 3$, the 3-D pillared layer architecture is persistent for a series of organodiammonium cations (type **4**). However, chain contraction to $n = 2$ results in a V−P−O 3-D framework (type **7**) as a result of the short spacer and the concomitant chelation mode adopted by the diphosphonate ligand. Curi-

(60) Stupp, S. I.; Braun, P. V. *Science* **1997**, *277*, 1242.

ously, lengthening of the tether length to $n = 5$ results in a 2-D pillared layer architecture (type **5**), reminiscent of that of type **2** oxides. When a piperazinium cation is present, a distinct 2-D structure, constructed from oxovanadium organophosphonate chains, is obtained (type **6**).

In view of the structural diversity of this compositionally simple series of oxides, the structural systematics of the V−P−O-based hybrid materials remain elusive, clearly reflecting the dynamic synergism between organic and inorganic components in the hydrothermal domain. While complete structural predictability remains elusive, recurrent structural motifs, as well as general strategies for the exploitation of organic components in the design of metal−oxide hybrid materials, continue to emerge. For example, the volume accessible to guest molecules in types **1** and **4** oxides may be tuned by the appropriate choice of the tether length and/or organic cation. The frameworks of these materials are relatively defect-free, and their porosities may be activated thermally, by dehydration, and/or by cation dissociation. The sorptive properties of the dehydrated materials of types **1′** and **4′** are under investigation.

**Acknowledgment.** This work was supported by grants from the National Science Foundation (Grant CHE0242153) and from the Defense Advanced Research Projects Agency (Grant MDA972-04-1-0029).

**Supporting Information Available:** TGA profiles, IR data for **6c** and **6c′**, magnetic susceptibility plots, and X-ray crystallographic data (CIF). This material is available free of charge via the Internet at http://pubs.acs.org.

IC0517422